NOTICE

The quality of this microform is heavily dependent upon the quality of the original thesis submitted for microfilming. Every effort has been made to ensure the highest quality of reproduction possible.

If pages are missing, contact the university which granted the degree.

Some pages may have indistinct print especially if the original pages were typed with a poor typewriter ribbon or if the university sent us an inferior photocopy.

Reproduction in full or in part of this microform is governed by the Canadian Copyright Act, R.S.C. 1970, c. C-30, and subsequent amendments.

AVIS

La qualité de cette microforme dépend grandement de la qualité de la thèse soumise au microfilmage. Nous avons tout fait pour assurer une qualité supérieure de reproduction.

S'il manque des pages, veuillez communiquer avec l'université qui a conféré le grade.

La qualité d'impression de certaines pages peut laisser à désirer, surtout si les pages originales ont été dactylographiées à l'aide d'un ruban usé ou si l'université nous a fait parvenir une photocopie de qualité inférieure.

La reproduction, même partielle, de cette microforme est soumise à la Loi canadienne sur le droit d'auteur, SRC 1970, c. C-30, et ses amendements subséquents.

TRUE TIME DOMAIN BANDPASS BEAMFORMING

by

Dion C. M. Horvat

B.A.Sc., Simon Fraser University, 1988

A THESIS SUBMITTED IN PARTIAL FULFILLMENT

OF THE REQUIREMENTS FOR THE DEGREE OF

MASTER OF APPLIED SCIENCE (ENGINEERING SCIENCE)

in the School

of

Engineering Science

Simon Fraser University

November, 1990

ISBN 0-315-69429-7

Canada

APPROVAL

NAME: 'Dion C. M. Horvat

DEGREE: Master of Applied Science (Engineering Science)

TITLE OF THESIS: True Time Delay Bandpass Beamforming

EXAMINING COMMITTEE:

Chairman: Dr. Shawn Stapleton

Dr. John Bird
Senior Supervisor

Dr. Steve Hardy
Supervisor

Dr. Jim Cavers
Supervisor

Dr. Paul Ho
Supervisor

Dr. Jacques Vaisey
Examiner

DATE APPROVED: December 6, 1990

PARTIAL COPYRIGHT LICENSE

I hereby grant to Simon Fraser University the right to lend my thesis, project or extended essay (the title of which is shown below) to users of the Simon Fraser University Library, and to make partial or single copies only for such users or in response to a request from the library of any other university, or other educational institution, on its own behalf or for one of its users. I further agree that permission for multiple copying of this work for scholarly purposes may be granted by me or the Dean of Graduate Studies. It is understood that copying or publication of this work for financial gain shall not be allowed without my written permission.

Title of Thesis/Project/Extended Essay

"True Time Domain Bandpass Beamforming"

Author: _____
(signature)

Dion C. Horvat
(name)

Dec 6 '95
(date)

Abstract

This thesis presents a simple digital scheme for a bandpass time-domain beamformer that can be realized using a single analog-to-digital converter and two short finite impulse response filters. The three processes required to obtain complex-baseband beam signals, namely, down conversion to complex baseband, time delay of the complex envelope, and phase rotation, are discussed. Down conversion is accomplished by subsampling the bandpass signal and an efficient interpolation technique is employed to time register these samples. This same interpolation technique is also used to obtain the time delays required for beamforming, hence the down conversion and signal delay are combined into a single process.

This new beamforming technique was tested experimentally in an underwater acoustic environment. The beamformer was successful in combining signals from arrays with closely spaced hydrophones and arrays where the hydrophones were spaced far apart. This beamforming technique is not restricted to sonar, but can be applied in other areas where antenna arrays are used, such as radar.

Acknowledgements

I would like to thank Dr. John Bird for his assistance and guidance throughout the course of this research. I would also like to thank the other URL members: Martic, Harry, Ian, Bill, and William. Finally, I thank Simrad Mesotech for the generous use of their facilities.

Contents

List of Figures

Chapter 1

Introduction

1.1 Background and Motivation for Research

1.1.1 Beamforming, The Concept

Due to the severe attenuation of electromagnetic radiation in water, the acoustic channel is the only practical means for communicating underwater over any reasonable distance. Unfortunately, the underwater acoustic channel is a very reverberant environment resulting in a considerable amount of multipath interference which interferes with the direct arrival and corrupts the message. Consider a ship at the surface communicating with an autonomous underwater vehicle (AUV) as shown in Figure 1.1. The AUV receives a direct signal followed by a surface reflection and a bottom reflection. The strengths of the reflected signals and their arrival times depend on the environment and the orientation of the vehicle.

The problem of multipath interference can be suppressed by using an array of hydrophones. The array has a greater spatial selectivity than a single hydrophone

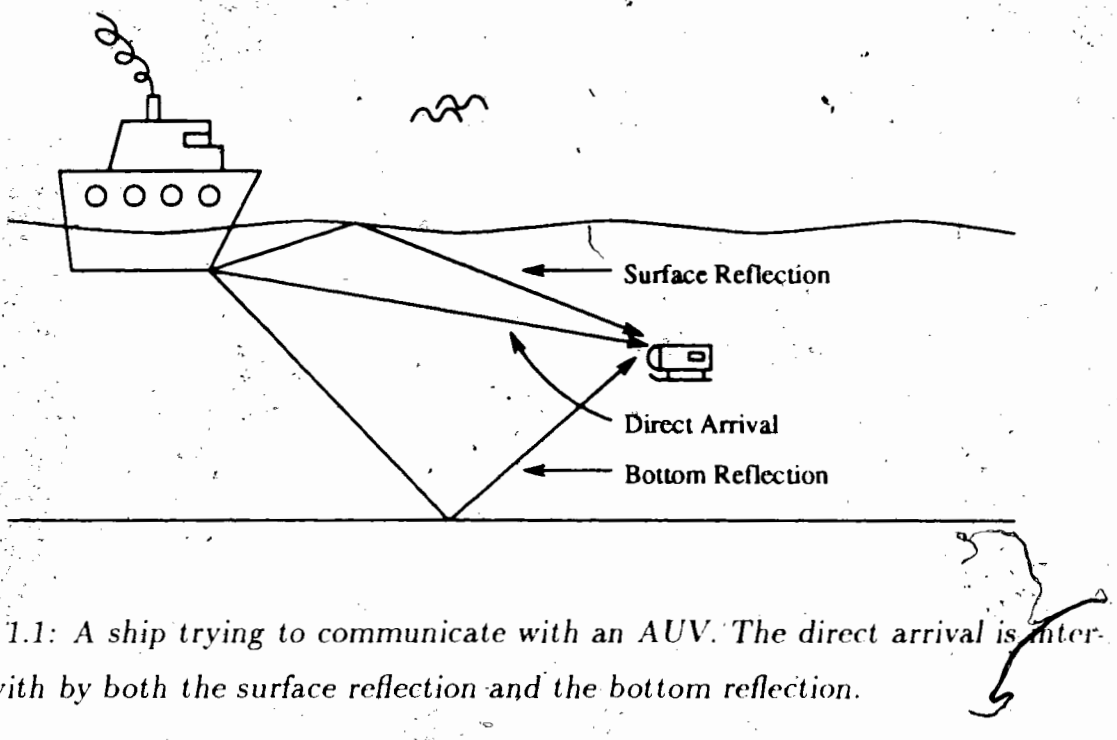

Figure 1.1: A ship trying to communicate with an AUV. The direct arrival is interfered with by both the surface reflection and the bottom reflection.

and therefore enhances the direct signal while suppressing the reflected signals. The array's effect on signal quality has been studied and documented by Radziejewski [1]. Compared to the signal received on a single hydrophone, it was found that the magnitude of the multipath arrivals are reduced by as much as 20 dB, with an array consisting of just three hydrophones.

As a signal travels across the array, there is a time delay between its arrival at each hydrophone as shown in Figure 1.2. The time delays depend on the orientation of the array and signal direction. Beamforming is the process by which the hydrophone signals are combined to reinforce a signal from a desired direction. To do this, the signal at each hydrophone is shifted in time so that it lies on a plane that is perpendicular to the beam direction and passes through a reference point. For the example in Figure 1.2, the reference point is chosen to be Hydrophone 2. In Figure 1.2(a), the signal is broadside to the array and there is no time delay between the signal arriving at each of the hydrophones. In order to enhance the received signal, the signal from the

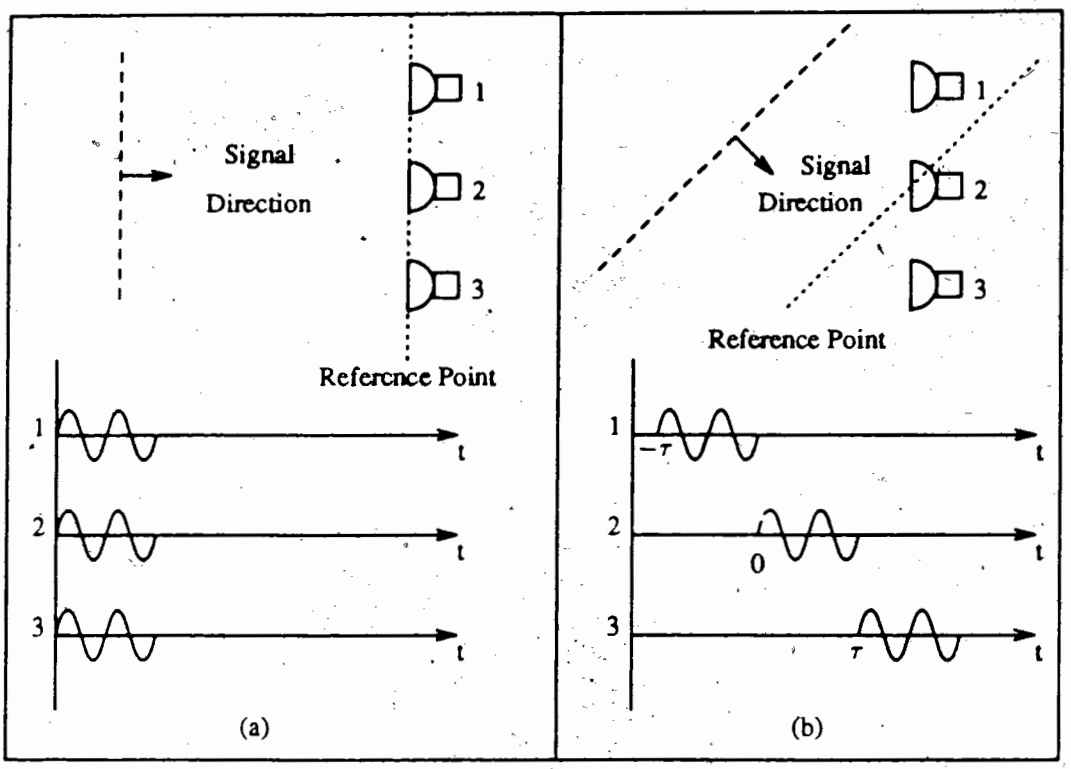

Figure 1.2: a) The signal is broadside to the array and arrives at each of the hydrophones at the same time. b) The signal is travelling across the array at an angle and there is a time delay between its arrival at each hydrophone.

hydrophones are simply added together. In Figure 1.2(b), the signal is propagating across the array at an angle and there is a time delay, τ, between the signals arriving at each of the hydrophones. In order to enhance the desired signal, the signal at Hydrophone 1 must be delayed by τ, and the signal at Hydrophone 3 advanced in time by τ before they are combined. When the time shifted signals are combined (added together), the signal received from the selected direction is significantly enhanced relative to the signals arriving from other directions and to incoherent background noise.

1.1.2 Beamformer Requirements for AUV Communications

The beam pattern describes the spatial response of an array. Figure 1.3 shows the beam pattern obtained with a 3 hydrophone linear array with 1/2 wavelength el-

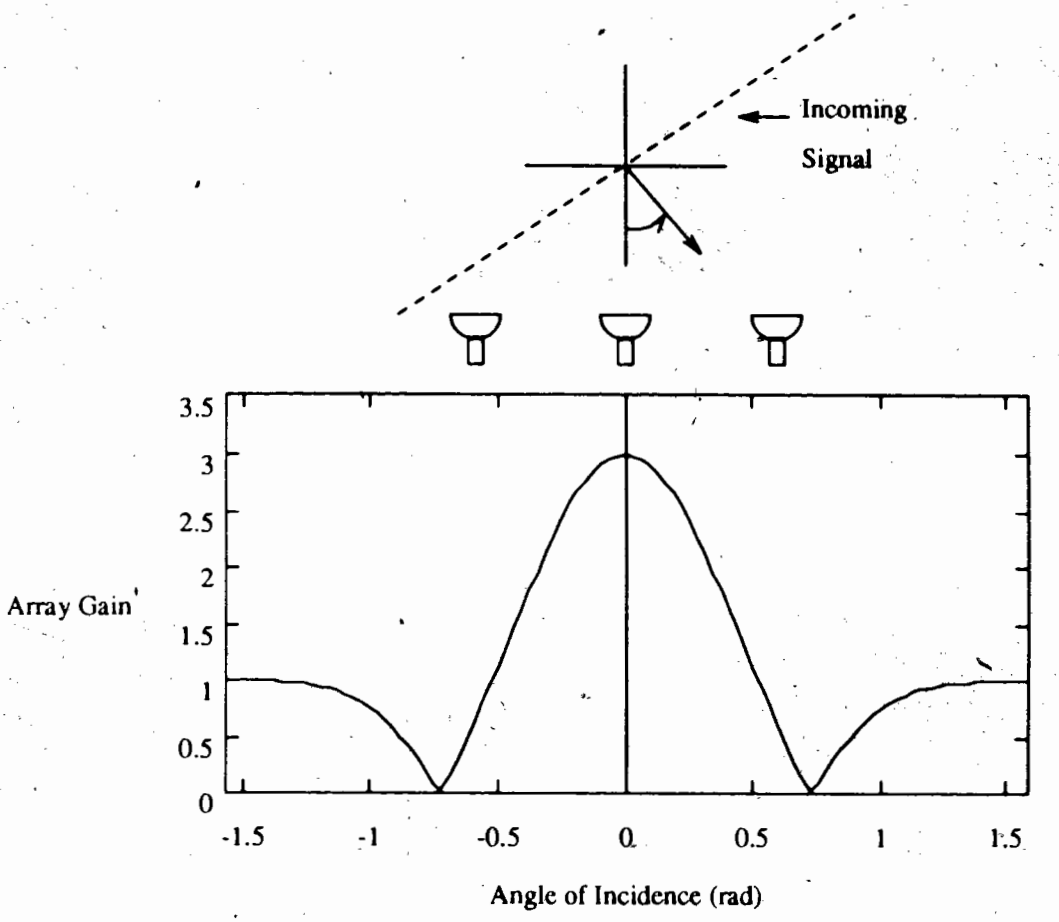

Figure 1.3: Array pattern for a 3-hydrophone array. The hydrophone spacing is $\lambda/2$ where λ is the wavelength.

ement spacing when the signals from each hydrophone are simply added together. Radziejewski [1] found that when the direct arrival was outside the main lobe (centred at 0° for this array) of the array pattern, the ratio of the direct signal's energy over the reflected signal's energy was poor. Only in the case where the transmitter and

receiver were in fixed locations relative to one another, and also aligned for optimum reception, was a fixed array advantageous. These results demonstrate the necessity of being able to continuously steer the array's 'look direction' when communicating with a moving target, such as an AUV.

When the array is used to improve the spatial selectivity of a receiver, the hydrophones are usually spaced at a half wavelength or less, as in Figure 1.3, to prevent the occurrence of grating lobes (large-amplitude lobes in the beam pattern at directions other than the steered direction) [2, 3]. There are, however, instances when it is not necessary to form a single narrow beam but rather just to facilitate the coherent combining of a direct arrival such as in a coherent spatial diversity receiver. Such a spatial diversity receiver uses an arbitrary or random array whose hydrophones are spaced far apart relative to the signal's wavelength [4]. For example, Catipovic [5] used two hydrophones spaced 20 m apart to implement a 10 kbps underwater communications system. Regardless of the application however, the same signal processing must be performed on the signals from the hydrophones before they are coherently combined. Namely, the beamformer must take into account the propagation delay of the wavefront incident onto the array.

Another instance where an arbitrary array is used, specific to communicating with an AUV, is on the AUV itself. To reduce drag, the placement of the hydrophones should conform to the AUV's body, hence, the beamformer must handle an arbitrary array.

Modulated bandpass signals are used for underwater acoustic communications because acoustic transducers are bandpass radiators which operate at centre frequencies higher than the message bandwidth. Also, the centre frequencies must be high enough to obtain efficient radiation with a transducer of reasonable dimensions. Therefore, the beamformer is required to process bandpass signals.

In summary, the beamformer's requirements for communicating with an AUV are:

- A continuously steerable beam
- Able to handle arbitrary or random arrays
- Processes bandpass signals

1.1.3 Previous Beamforming Techniques

Several techniques have been developed for beamforming. The earliest beamformers used analog delay lines to delay the incoming signals. However, there are problems associated with this technique. First, there is the uncertainty of component values and therefore a loss in the accuracy of the achievable delay times. Second, the stability of the delays due to changes in the working environment, such as temperature, is limited. Also, large delays, common with underwater arrays, are difficult to achieve. Lastly, to obtain many beams, there must be several delay lines for each hydrophone to effect the necessary delays. This obviously increases the complexity and size of the beamformer.

With the advent of modern digital signal processors, many beamforming methods have been developed that use digital techniques. However, as will be seen, the current techniques are less than ideal for communicating with an AUV. In fast Fourier transform (FFT) beamforming, the signal from each hydrophone is first converted to the frequency domain by performing a discrete Fourier transform (DFT), then phase shifting of the separate frequency bins (accomplished by a second DFT) is employed to realize the required time delays [6, 7, 8, 9, 10, 11]. While this approach does offer several advantages, such as creating several look directions simultaneously and efficiently, it has its drawbacks for our application. For example, the second DFT requires that the time delay for the signal to propagate between adjacent hydrophones be the same, hence, FFT beamforming will only work with linear arrays and not arbitrary or random arrays. Also, the number of beams available depends on the frequency, hence FFT beamforming does not work well for broadband signals.

For communication systems, the output is usually required to be in the time domain, therefore an inverse transform is required, which serves to increase the computational load. Finally, phase shifting each frequency bin by multiplying it by a complex exponential effectively revolves the signal in the time domain about itself. That is, the signal is circularly convolved with a delayed impulse, hence, instead of the signal near the edge of a block being shifted out, it appears in the same block but near the other edge. This results in the full array gain not being achieved and is known as edge effects.

Beamforming techniques that operate in the time domain are called time-domain beamformers. Unlike FFT beamformers, time-domain beamformers can handle arbitrary or random arrays. They also process a steady stream of data rather than data blocks, hence they are not plagued by edge effects. The earliest digital time-domain beamformers could form delays composed only of an integer number of sample periods and the beams were limited to what is known as a synchronous beam set. To have a steerable look direction, the signal has to be grossly oversampled, thus increasing the requirements of the analog-to-digital converter (A/D) and the cable and amplifier bandwidths. For large arrays, the required time delays may be such that the amount of memory required to store the samples could be overwhelming. When the signal is a bandpass signal, a separate demodulator is necessary in order to demodulate the signal to baseband.

The requirement on the sampling frequency is greatly reduced by employing interpolation techniques to realize the time delays [12]. Interpolation provides an arbitrary delay without the overhead of many unused samples although the signal is still required to be sampled at the Nyquist rate to prevent aliasing. However, interpolation only provides an estimate of the signal and steps have to be taken to ensure that the interpolation error is small.

Another beamformer, common with bandpass signals, simply phase rotates the

complex envelope [13]. The complex envelope is a complex baseband signal consisting of the inphase and quadrature components of a bandpass signal. The inphase signal is the real part of the complex envelope and the quadrature signal is the imaginary part. To account for the time delay, the phase-rotation beamformer rotates the phase of the complex envelope from each of the hydrophones before adding the signals together. Since the phase rotation can realize any time delay, it can provide a continuously steerable beam as well as work using arbitrary or random arrays. However, for the phase-rotation beamformer to be effective; there must be sufficient overlap in time of the complex envelopes from each of the hydrophones in the array. Phase-rotation beamformers work well in radar applications, where the incoming signals propagate at the speed of light ($\approx 3X10^8$ m/s) and hence the time delay between the signal arriving at the various elements of an array is often negligible compared to the time for a significant change in the complex envelope. In this case the complex envelopes are aligned in time and just have to be phase rotated to be coherently combined. In sonar, however, the speed of the acoustic signal in water ($\approx$ 1500 m/s) is much slower and the delay between the signal at the hydrophones may be large compared to the time for a significant change in the complex envelope. In such cases, there is not sufficient overlap of the complex envelopes from each hydrophone for the signals to add together without the resulting signal being significantly distorted.

In chapter 2, the above beamforming techniques are described in more detail, along with the reasons why they are not suitable for communicating with an AUV.

1.1.4 True Time Delay Bandpass Beamforming

This thesis presents a time-domain beamforming method that combines in a unique way the beamforming technique described by Pridham and Mucci [14] with the optimum interpolation method of Oetken [16]. The bandpass signal from each of the hydrophones is first converted to its complex envelope representation using a tech-

nique known as bandpass sampling where the signal is actually subsampled with respect to the carrier frequency [17]. With a careful choice of the sampling frequency, the resulting samples are either of the inphase or the quadrature signal. The effects on the complex envelope of time delaying the bandpass signal are then realized so that the signals can be coherently combined. This involves both delaying and phase rotating the complex envelope.

The delay is realized by first delaying or advancing the signal the required number of integer sample periods and then using an efficient interpolation technique to estimate the signal for the required fraction of a sample period. The interpolation method is implemented using a finite impulse response (FIR) filter whose coefficients depend on the point where the signal is to be interpolated to. This interpolation technique requires a fewer number of filter taps than other commonly used interpolation techniques to obtain a low interpolation error. The phase rotation is executed by linearly combining the delayed inphase and quadrature signals after multipling them by values which depend on the time delay. The delayed and phase rotated signals from each of the hydrophones are then added together to construct the beamformer's output.

This new beamformer has several advantages over other digital beamformers for communicating with an AUV. First, since it has the ability to realize any time delay, it can handle random or arbitrary arrays as well as have a continuously steerable beam, both are unattainable with FFT beamforming. Second, unlike FFT beamforming, the signal remains in the time domain which makes it attractive for communication purposes. Also, by bandpass sampling the signal, the sampling frequency is greatly decreased over that normally required when sampling at the Nyquist rate for the bandpass signal. Having a low sampling rate not only reduces the analog-to-digital converter requirements but also reduces the the amount of memory necessary for realizing large delays.

The implementation of the new beamforming technique is simple and consists of an A/D converter, which may be shared between hydrophones, and two short FIR filters (≈20 taps) for each hydrophone in the array. The look direction is steered by changing the time delay for the signal from each hydrophone. To accomplish this, only the integer number of sample periods that the signal is delayed and the interpolation filter coefficients have to be changed. To have several separate simultaneous beams, several beamformers can be employed, each with a different look direction. This implementation has the advantage of soft degradation, unlike FFT beamforming; if one of the beamformers fails the rest will continue to operate.

The new beamforming technique was implemented on a Sun Sparc station and tested using real data collected with various array configurations. Both a small array and a large array were employed to demonstrate the beamformer's validity.

1.2 Thesis Outline

This thesis is divided into six chapters. Chapter 2 contains a discussion of both frequency-domain and time-domain beamforming techniques and their associated problems. The requirements, for beamforming using the complex envelope, are also stated.

In Chapter 3, techniques to recover the complex envelope are described. The beamformer can be simplified to perform as a quadrature demodulator. This demodulator is useful apart from the beamforming context and therefore is described in detail. The method uses bandpass sampling to down convert the bandpass signal and interpolation to time register the samples. Several interpolation techniques are investigated and results are given comparing their accuracy. The chosen interpolation technique is optimized to minimize the mean squared error of the interpolated signal.

Chapter 4 describes the proposed beamforming technique which performs the beamforming process on the complex envelope. The demodulation technique described in chapter 3 is employed with only a simple modification to effect the required time delay and phase rotation of the complex envelope.

Chapter 5 contains a design example and experimental results. Following the description of the test environment, results using various array configurations are given which confirm the beamformer's operation. Three trials were conducted, two with a small array and one with a large array. For the small array, the incident angles for the signal were 0^o and 30^o. The setup for the large array was such that there was little overlap in time of the complex envelope from each hydrophone. This illustrates the advantage the new technique has over phase-rotation beamformers.

The conclusions drawn from the research are discussed in Chapter 6.

Chapter 2

Beamforming

As mentioned in the introduction, an array of hydrophones will improve the spatial selectivity over that of a single hydrophone. As a signal propagates across the array, there is a time delay between the signal arriving at each hydrophone in the array. The time delays depend on the incident angle of the signal to the array. By properly taking into account the propagation delays, a signal from a particular direction is enhanced over signals from other directions and background noise. This process is called beamforming.

Beamforming can be accomplished using analog phase shifters or delay lines. However, analog beamformers suffer the problems associated with analog components. That is, the tolerances and stability of the components reduce the accuracy of the delays available. Also, in order to obtain a number of beams, many delay lines are required. Modern digital signal processing techniques and hardware eliminate many of the accuracy and stability problems associated with the analog beamformer. However, current digital beamforming techniques are not without their own weaknesses.

2.1 Digital Beamforming

Digital beamformers can be divided into two classes, time-domain beamformers and frequency-domain beamformers. Both classes will now be discussed.

2.1.1 Frequency Domain Beamformers

Frequency-domain beamformers first convert the signal from each hydrophone to the frequency domain by performing a discrete Fourier transform (DFT). The equation for the DFT of M samples of a signal, $x_i(n)$ $(n = 0, 1, \cdots, M-1)$, is [18]

$$X_i\left(\frac{2\pi k}{M}\right) = \sum_{n=0}^{M-1} x_i(n) e^{-j\frac{2\pi}{M}nk} \tag{2.1}$$

To ease the computational load, equation (2.1) is calculated using a fast Fourier transform (FFT) which computes $X_i\left(\frac{2\pi k}{M}\right)$ efficiently for $k = 0, 1, 2, \cdots, M-1$. Each value of the bin number k represents a different frequency and the relationship between k and the temporal frequency is

$$f_k = \frac{k}{M} f_s \tag{2.2}$$

where f_s is the sampling frequency.

Before combining the signals from the hydrophones in the array, each signal must be appropriately shifted in time so that they are aligned in time. As an example, consider a two hydrophone array where the signal reaches hydrophone 0 after hydrophone 1 as shown in Figure 2.1(a). The spectrum of each signal will have the same magnitude but different phase. That is, if the DFT of the signal at hydrophone 0 is

$$X_0\left(\frac{2\pi k}{M}\right) = A\left(\frac{2\pi k}{M}\right) e^{j\Phi\left(\frac{2\pi k}{M}\right)} \tag{2.3}$$

then the spectrum of the signal at hydrophone 1 will be

$$X_1\left(\frac{2\pi k}{M}\right) = A\left(\frac{2\pi k}{M}\right) e^{j\left(\Phi\left(\frac{2\pi k}{M}\right) + \left(\frac{2\pi k}{M} \tau f_s\right)\right)} \tag{2.4}$$

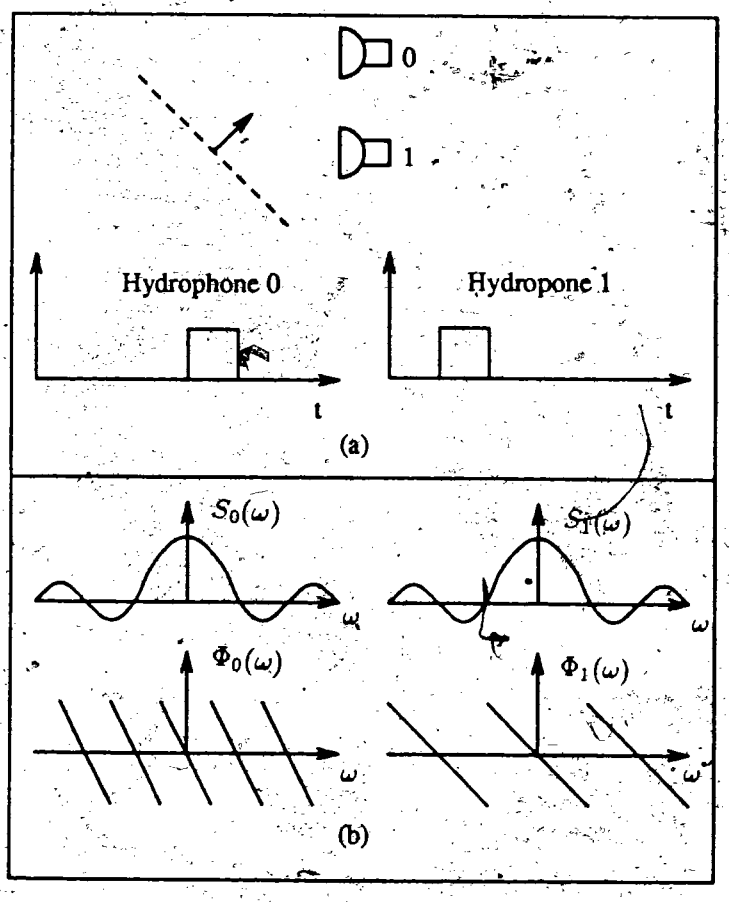

Figure 2.1: Signal arriving at two hydrophones (a) in the time domain (b) and in the frequency domain.

$$= A\left(\frac{2\pi k}{M}\right) e^{j\Phi(\frac{2\pi k}{M})} e^{j(\frac{2\pi k}{M}\tau f_s)} \tag{2.5}$$

where τ is the time difference for the signal to arrive at each hydrophone. To align both signals, the signal at hydrophone 1 must be delayed by τ which is implemented by multiplying $X_1(\frac{2\pi k}{M})$ by $e^{-j\frac{2\pi k}{M}\tau f_s}$. The two spectra are then added together to form the beamformer's spectrum.

For the specific case of a linear array consisting of N hydrophones and a time delay of τ between between neighboring hydrophones, the spectrum of the beamformer's output is [6].

$$B\left(\frac{2\pi k}{M}, \tau\right) = \sum_{i=0}^{N-1} X_i\left(\frac{2\pi k}{M}\right) e^{-j\frac{2\pi k}{M}\tau i f_s} \tag{2.6}$$

If equation (2.6) can be written in the form of a DFT, then it can be efficiently computed using an FFT. To write equation (2.6) as a DFT, the following substitution must be made

$$f_s \frac{\tau k}{M} = \frac{l}{N} \quad l = 0 \cdots (N-1) \tag{2.7}$$

The resulting equation for the beamformer's output is then

$$B\left(\frac{2\pi k}{M}, \frac{2\pi l}{N}\right) = \sum_{i=0}^{N-1} X_i\left(\frac{2\pi k}{M}\right) e^{-j\frac{2\pi}{N} l i} \tag{2.8}$$

which is a DFT and can be computed using an FFT.

The FFT beamformer can be visualized as shown in Figure 2.2. First, the signal from each hydrophone is transformed from the time domain to the frequency domain using an FFT. Each FFT creates M frequency bins for each hydrophone. Next the frequency bins are sorted according to the bin numbers, k, and the second DFT, equation (2.8), is computed to appropriately phase shift and add the signals.

FFT beamforming has drawbacks that restricts its use. The first problem is evident in equation (2.6). In order to compute the second DFT, the time delay for the signal to propagate between neighboring hydrophones, τ, must be the same for

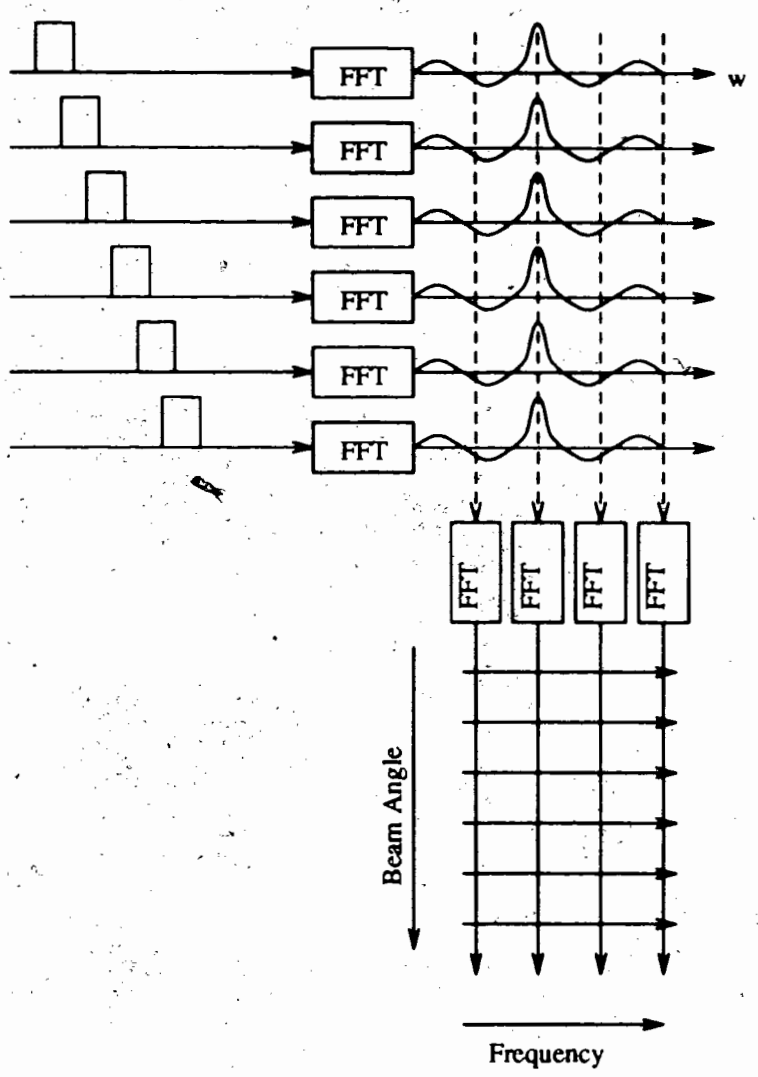

Figure 2.2: Visual representation of FFT beamforming.

all hydrophones. This means the hydrophones in the array must be evenly spaced (i.e., a linear array), hence, FFT beamforming does not work for arbitrary or random arrays.

The second problem is introduced by using the DFT to time delay the signals by phase shifting the frequency bins. When the DFT of two signals are multiplied together, the signals in the time domain undergo circular convolution [18]. In the case of FFT beamforming, the second DFT equation is multiplying the DFT of the hydrophone signals with the DFT of a delayed impulse. In the time domain, the hydrophone signal is actually circular convolved with a delayed impulse. Consider the example shown in Figure 2.3(a) where a signal is incident onto a 3-element array. The signal from each hydrophone is shown in Figure 2.3(b). Before adding the signals together, the signals from hydrophones 2 and 3 must be advanced in time to be aligned with the signal at hydrophone 1. Figure 2.3(c) shows the signals after being divided into blocks for processing. When the signals in the block are time shifted by multiplying the DFT by a complex exponential, rather than the signal near the edge of the block being shifted out, it instead appears at the other end of the block as shown in Figure 2.3(d). This results in the signal near the edge of the block not being coherent with the signals from the other hydrophones. Therefore, when the signals are added together, the signals near the edge are not added coherently which causes distortion in the beamformed signal. This distortion is known as edge effects. Edge effects are always present but to what degree depends on the ratio of the length of the data block and the propagation time across the array. Mucci [9] recommends that the length of the data block be at least ten times the maximum propagation delay across the array.

The third problem with FFT beamforming is that the beam is not continuously steerable. The substitution in equation (2.7) limits the possible values for the delay τ and hence limits the look directions [10]. Using equation (2.7) and the fact that k represents the temporal frequency $f_k = kf_s/M$, the possible values for the delay τ

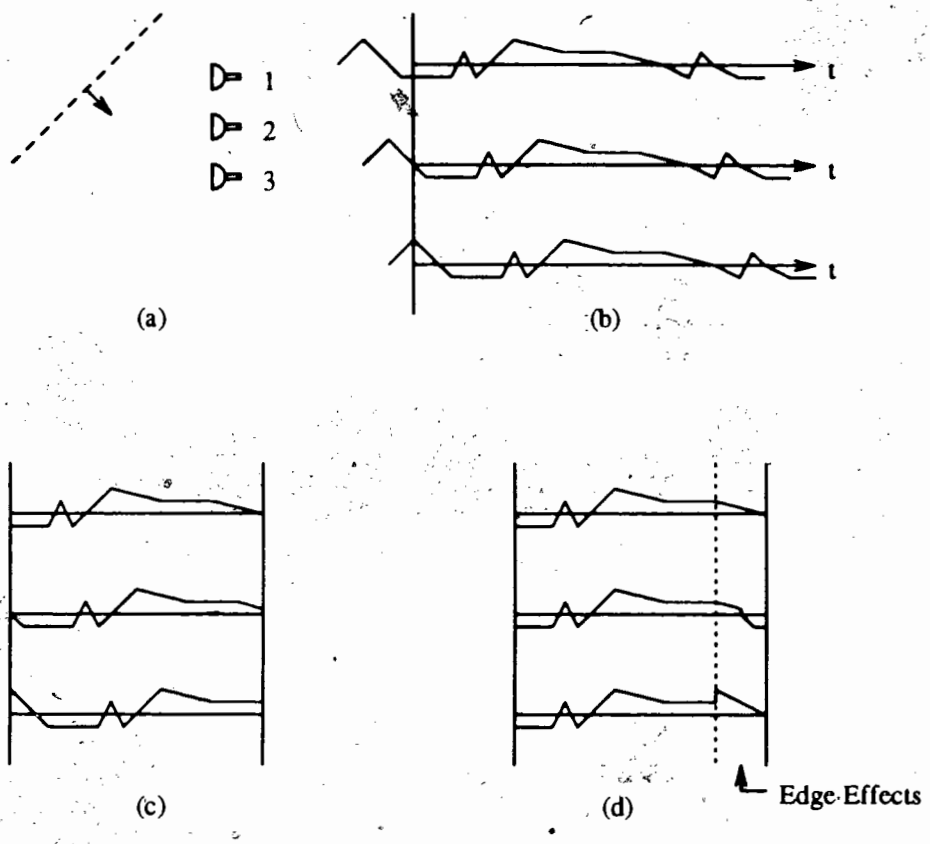

Figure 2.3: (a) Three hydrophone array with the signal coming in at an angle. (b) Signal at each of the hydrophones. (c) Signal at each of the hydrophones divided into a block. (d) Signal at each hydrophone after being circular convolved with a delayed impulse.

are

$$\tau = \frac{l}{Nf_k} \quad l = 0 \cdots (N-1) \tag{2.9}$$

For an incident angle of Θ, as shown in Figure 2.4, the time delay τ can be expressed

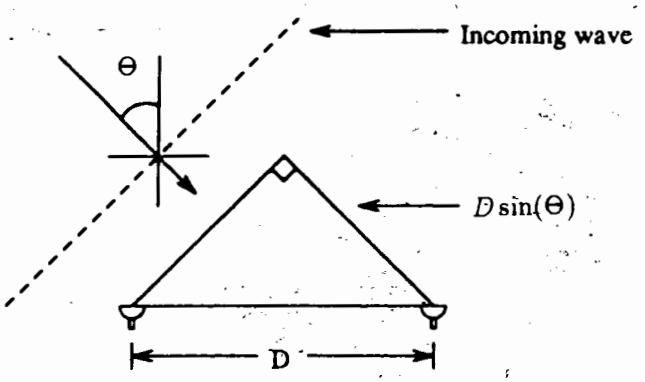

Figure 2.4: The extra distance a signal has to travel to reach the second hydrophone is $D\sin(\Theta)$. This corresponds to a time delay of $D\sin(\Theta)/v$.

as

$$\tau = \frac{D\sin(\Theta)}{v} \tag{2.10}$$

where v is the velocity of sound in water. Equating equations (2.9) and (2.10) results in the possible angles for the look direction

$$\Theta = \sin^{-1}\left(\frac{lv}{NDf_k}\right) \tag{2.11}$$

There are two points to note about the look directions angles expressed in equation (2.11). First, the beam direction is not continuously steerable but is incremented by discrete steps. Second, the look direction depends on the temporal frequency f_k. Having the look direction depend on frequency when the signal is wider than a single frequency bin is undersirable for communincations.

The final problem with FFT beamforming is the processed signal is in the frequency domain. If the output is required to be in the time domain, as it is for most

communication applications, an inverse transform is necessary further increasing the computational load for the beamformer. .

The main advantage of the FFT beamformer is its inherent ability to generate many beams efficiently. However, multiple beams are not required for communicating with an AUV and the problems associated with FFT beamforming certainly make it unattractive for our purposes.

2.1.2 Time-Domain Beamformers

Time-domain beamformers do not have the problems associated with FFT beamformers. The simplest time-domain beamformer is the delay-sum beamformer where the output is

$$b(nT_s) = \sum_{i=0}^{N-1} x_i(nT_s - \tau_i) \tag{2.12}$$

where τ_i is the required delay for hydrophone i. The early digital delay-sum beamformers could only form delays composed of integer multiples of the sampling period [3]

$$b(nT_s) = \sum_{i=0}^{N-1} x_i(nT_s - k_iT_s) \tag{2.13}$$

where k_i is an integer. Assuming an array whose hydrophones are evenly spaced, the requirement that the delays be integer multiples of the sampling period restrict the choice of beam angles to

$$\theta = \sin^{-1}\left(\frac{kT_s}{D/v}\right) \quad k = 0, \pm 1, \pm 2, \cdots \tag{2.14}$$

where D is the hydrophone spacing and v is the speed of sound. This beam set is referred to as a synchronous beam set. The obvious disadvantage of the direct approach of implementing the time delay is the high sampling rate required to obtain the time delayed signals needed to steer the beam. The large sampling rate increases the requirements of the A/D converter and the cable and amplifier bandwidths. Also,

a large amount of memory is required to achieve the long delays necessary for large arrays.

Instead of grossly oversampling the signal, interpolation can be employed to obtain the delayed signals [12]. Interpolation is preferred because any delay is attainable, and hence the beam is continuously steerable without the overhead of many unused samples. The reduced sampling rate also reduces the A/D requirements and the cable and amplifier bandwidths. However, the interpolators only provide an estimate of the signal and any error in the estimate is treated as noise. The use of interpolators therefore adds noise and steps must be taken to ensure the noise is small. Interpolation is discussed in detail in chapter 3.

If the received signal is a bandpass signal, the required output signal is often the complex envelope. Rather than beamform the bandpass signal and then use a separate method to recover the complex envelope, it is possible to perform the beamforming operation on the complex envelope. However, simply delaying the complex envelope before combining the signals is not sufficient, it must also be rotated in phase. Before demonstrating the necessity of phase rotating the complex envelope, a discussion of the complex envelope and its relationship to the bandpass signal is in order.

Complex Envelope

A bandpass signal, $x(t)$, can be represented using its inphase and quadrature components as

$$x(t) = I(t)\cos(\omega_c t) - Q(t)\sin(\omega_c t) \qquad (2.15)$$

where $I(t)$ and $Q(t)$ are the inphase and quadrature baseband signals respectively and ω_c is the carrier frequency.

The complex envelope of $x(t)$, denoted by $\tilde{x}(t)$, is defined as [19]

$$\tilde{x}(t) = (x(t) + jx_H(t))e^{-j\omega_c t} \tag{2.16}$$

where $x_H(t)$ is the Hilbert transform of $x(t)$. Equation (2.16) can be simplified resulting in an equation for the complex envelope in terms of the quadrature components

$$\tilde{x}(t) = I(t) + jQ(t) \tag{2.17}$$

The complex envelope is a complex baseband signal whose real part is the inphase signal and imaginary part is the quadrature signal.

Beamformed Complex Envelope Requirements

The requirements of delaying and phase rotating the complex envelope when the beamformer processes the complex envelope will now be demonstrated. Again the equation for the bandpass signal at hydrophone i is

$$x_i(t) = I_i(t)\cos(\omega_c t) - Q_i(t)\sin(\omega_c t) \tag{2.18}$$

If the signals from the hydrophones are to be coherently combined at baseband, the beamformer must be able to accomplish the effect of a time delay of a bandpass signal. Specifically, it must determine the inphase and quadrature signals for a delayed bandpass signal.

If the bandpass signal in (2.18) is delayed by τ_i then

$$x_i(t-\tau_i) = I_i(t-\tau_i)\cos(\omega_c(t-\tau_i)) - Q_i(t-\tau_i)\sin(\omega_c(t-\tau_i)) \tag{2.19}$$

After expanding the trigonometric functions and combining terms

$$x_i(t-\tau_i) = I_{Di}(t)\cos(\omega_c t) - Q_{Di}(t)\sin(\omega_c t) \tag{2.20}$$

where

$$I_{Di}(t) = I_i(t-\tau_i)\cos(\omega_c\tau_i) + Q_i(t-\tau_i)\sin(\omega_c\tau_i) \tag{2.21}$$

and

$$Q_{Di}(t) = -I_i(t-\tau_i)\sin(\omega_c\tau_i) + Q_i(t-\tau_i)\cos(\omega_c\tau_i) \tag{2.22}$$

$I_{Di}(t)$ and $Q_{Di}(t)$ are the new inphase and quadrature baseband signals that represent the delayed bandpass signal. These may be added to delayed baseband signals from the other elements to form the baseband beam output.

Three distinct processes are necessary to obtain the requisite baseband output as shown in equations (2.21) and (2.22). First, the bandpass signal must be down converted to obtain the inphase and quadrature baseband signals. Second, the baseband signals must be delayed by τ_i. Finally, the baseband signals must be rotated in phase (linear combination of I_i and Q_i multiplied by $\cos(\omega_c\tau_i)$ and $\sin(\omega_c\tau_i)$).

There is a beamforming technique (phase-rotation beamforming) where the quadrature signals of the delayed bandpass signal are estimated to be [13]

$$I_{Di}(t) \approx I_i(t)\cos(\omega_c\tau_i) + Q_i(t)\sin(\omega_c\tau_i) \tag{2.23}$$

and

$$Q_{Di}(t) \approx -I_i(t)\sin(\omega_c\tau_i) + Q_i(t)\cos(\omega_c\tau_i) \tag{2.24}$$

The beamformer rotates the complex envelope but does not delay it. These beamformers work well when the propagation time across the array is small compared to the time it takes for a significant change in the complex envelope. Consider the example shown in Figure 2.5 where the time delay between the signal arriving at each hydrophone is small. When demodulated to the complex envelope, the signals appear to be closely aligned in time but the complex envelopes need to be rotated in phase so that they can be coherently combined, Figure 2.5(a). The phase-rotation beamformer simply rotates the complex envelopes before summing the signals, forming the enhanced signal Figure 2.5(b). In this case the signal at hydrophones 2 and 3 are rotated in phase and added to the signal at hydrophone 1. If the time delay is small, the distortion in the beamformed signal is small.

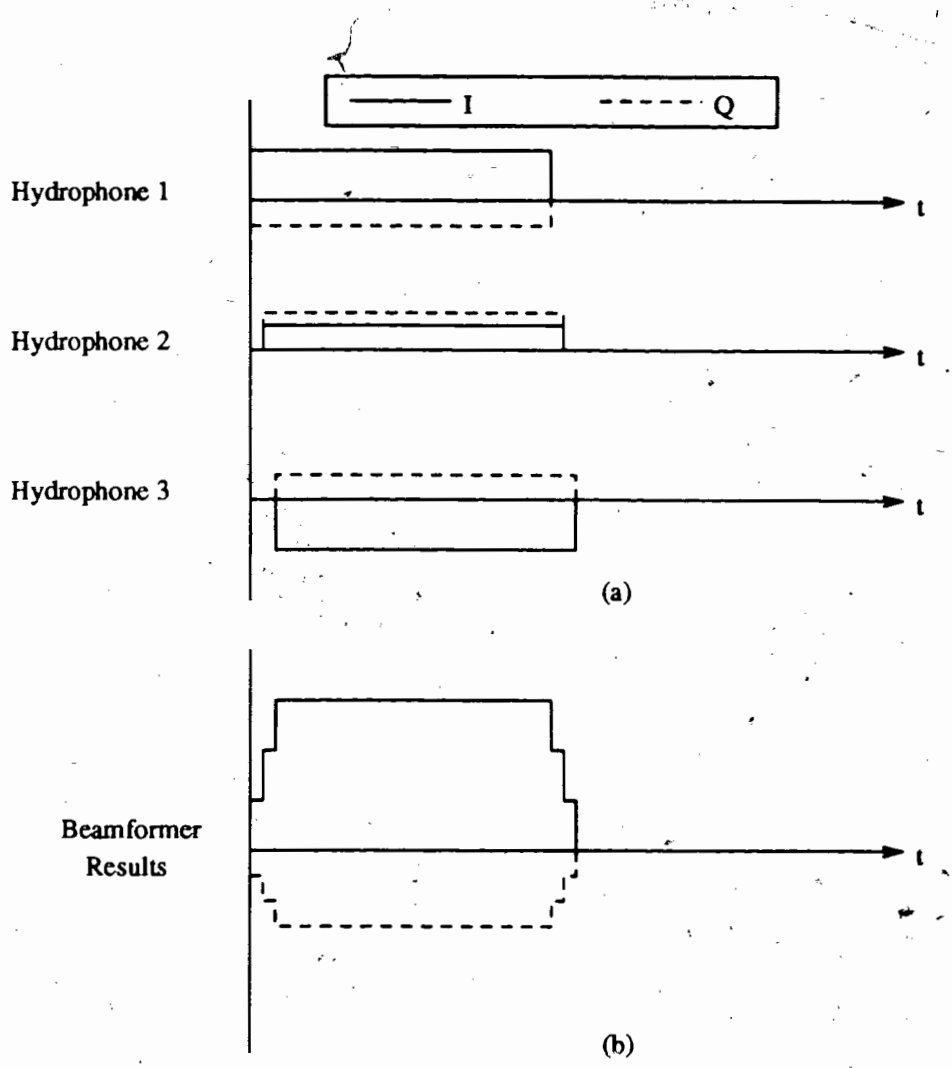

Figure 2.5: A situation where the time delay between the signal arriving at each hydrophone is small and phase-rotation beamforming works well. (a) Complex envelope at each hydrophone. (b) Phase-rotation beamformed signal.

Now consider the example shown in Figure 2.6 where the time delay between the

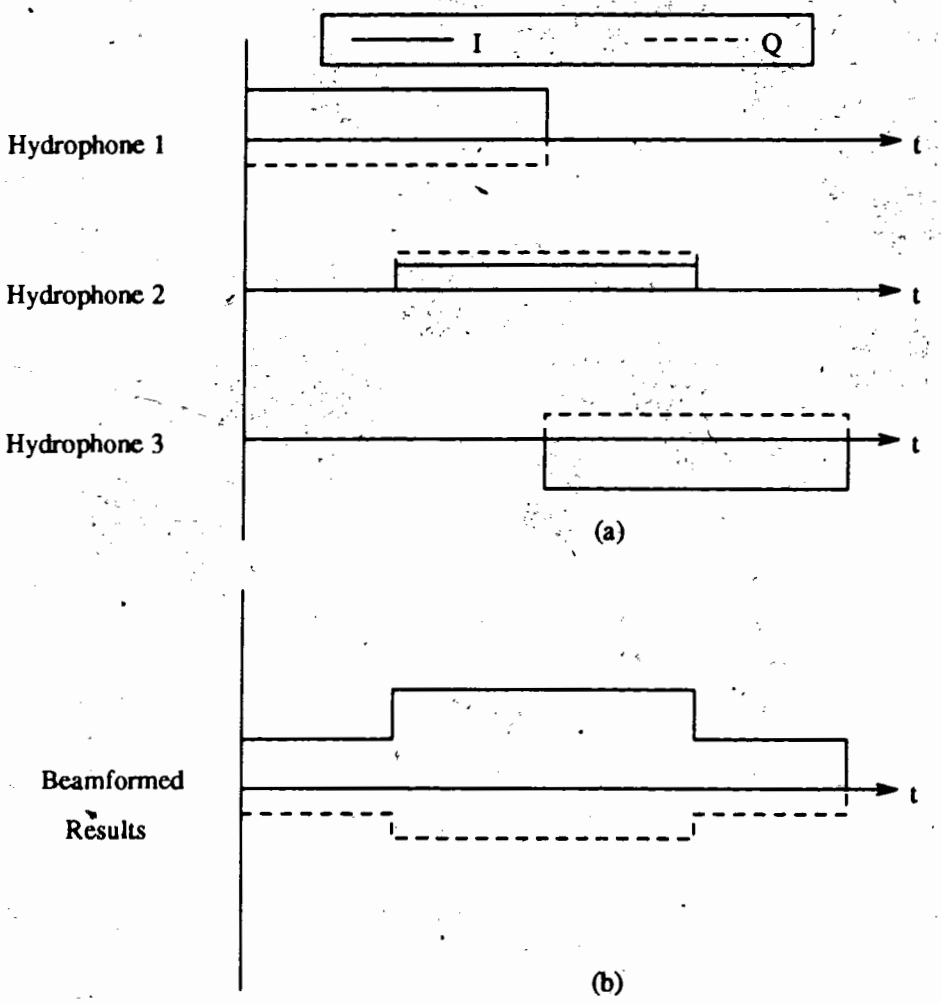

Figure 2.6: A situation where the time delay between when the signal arrives at each hydrophone is large and phase-rotation beamforming does not works well. (a) Complex envelope at each hydrophone. (b) Phase-rotation beamformed signal.

signal arriving at each hydrophones is large. Again, the complex envelope at each hydrophone needs to be rotated in phase before being added together. However, adding the phase rotated signals results in a seriously distorted signal, Figure 2.6(b). To prevent distortion, the signals need to be time delayed also.

A means to limit the amount of distortion that phase-rotation beamformers cause is to restrict the amount the signal changes between the first and last hydrophone in the array. If for an N element array, the baseband signals at each hydrophone, after being phase rotated, are $y(t)$, $y(t-\tau_1)$, $y(t-\tau_2)$, $\cdots$, $y(t-\tau_{N-1})$, then the beamformed signal is

$$b(t) = y(t) + y(t-\tau_1) + y(t-\tau_2) + \cdots + y(t-\tau_{N-1}) \tag{2.25}$$

The desired signal is $Ny(t)$, so the absolute value of the error is

$$\epsilon = \mid Ny(t) - y(t) - y(t-\tau_1) - y(t-\tau_2) - \cdots - y(t-\tau_{N-1}) \mid \tag{2.26}$$

$$\epsilon = \mid (N-1)y(t) - y(t-\tau_1) - y(t-\tau_2) - \cdots - y(t-\tau_{N-1}) \mid \tag{2.27}$$

Assuming that $\mid y(t) - y(t-\tau_i) \mid$ is largest for i equal to $N-1$, then

$$\epsilon \leq (N-1) \mid y(t) - y(t-\tau_{N-1}) \mid \tag{2.28}$$

We want to restrict the expected mean squared value of ϵ to a fraction, A, of the desired signal's power

$$\mathrm{E}[\epsilon^2] \leq (N-1)^2 \mathrm{E}[(y(t) - y(t-\tau_{N-1}))^2] \leq AN^2 \mathrm{E}[y(t)^2] \tag{2.29}$$

from which the following equation is written

$$\mathrm{E}[(y(t) - y(t-\tau_{N-1}))^2] \leq A \left(\frac{N}{N-1}\right)^2 \mathrm{E}[y(t)^2] \tag{2.30}$$

Papoulis [20] derived the following inequality

$$\mathrm{E}[(y(t) - y(t-\tau_{N-1}))^2] \leq \omega_m^2 \tau_{N-1}^2 \mathrm{E}[y(t)^2] \tag{2.31}$$

where ω_m is the highest frequency in $y(t)$. If the inequality

$$\omega_m^2 \tau_{N-1}^2 \mathrm{E}[y(t)^2] \leq A \left(\frac{N}{N-1}\right)^2 \mathrm{E}[y(t)^2] \tag{2.32}$$

is true, then the inequality in (2.30) will also be true. For (2.32) to hold, the equation limiting the maximum propagation delay is

$$\tau_{N-1} \leq \frac{N\sqrt{A}}{(N-1)\omega_m} \text{ (s)} \tag{2.33}$$

For an array of length L m, the maximum propagation delay occurs when the incident angle for the signal is 90^O (i.e., endfire). The maximum propagation delay is

$$\tau_{N-1}(\text{max}) = \frac{L}{1500} \text{ (s)} \tag{2.34}$$

where 1500 m/s is the speed of sound in water. An equation limiting the length of the array is obtained by substituting equation (2.34) into (2.33) and solving for L

$$L \leq \frac{1500N\sqrt{A}}{(N-1)\omega_m} \text{ (m)} \tag{2.35}$$

As an example, consider a two element array and the signal bandwidth is 12600 rad/sec. For the error to be 40 dB down (A=0.0001), the maximum length of the array is 2.4 cm.

The true time delay bandpass beamformer described in this thesis overcomes this problem by delaying as well as phase rotating the complex envelope.

Chapter 3

Quadrature Demodulation

Down converting a bandpass signal to its complex envelope is known as quadrature demodulation and several methods, both analog and digital, have been developed to accomplish this. This chapter presents some of these methods. The proposed beamforming process can be simplified to perform as a quadrature demodulator. Since the demodulator is useful apart from the beamforming context, this simplification is discussed in detail.

3.1 Previous Demodulation Techniques

A conventional approach to demodulate a bandpass signal into samples of $I(t)$ and $Q(t)$ is shown in Figure 3.1 [17, 21, 22, 23]. The demodulator consists of two quadrature channels that mix the bandpass signal down to baseband. Two A/D converters then sample $I(t)$ and $Q(t)$ to generate the digitized outputs. The most significant problem with this approach is balancing both the gain and the phase between the two channels. A typical phase error for this type of demodulator is in the order of 2° to 3° [22]. Various other schemes using digital signal processing techniques

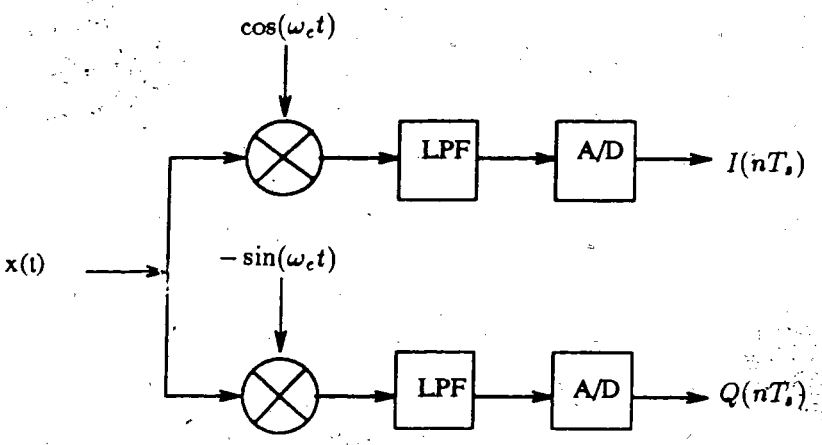

Figure 3.1: A conventional quadrature demodulator.

have been developed to improve the quadrature demodulator's performance.

Equation (2.16) suggests using the Hilbert transform to quadrature demodulate a bandpass signal [18, 17]. The block diagram in Figure 3.2 illustrates an implementation of a quadrature demodulator using the Hilbert transform. The signal spectrum

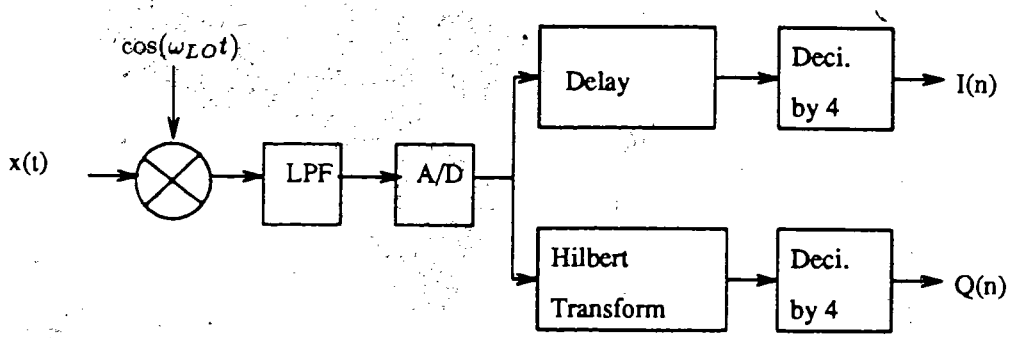

Figure 3.2: A quadrature demodulator using the Hilbert transform.

at various points in the demodulator is shown in Figure 3.3. In this approach, the bandpass signal, Figure 3.3(a), is first mixed down to an IF signal centred at f_b, Figure 3.3(b), and then sampled at a rate of $4f_b$, Figure 3.3(c). The samples are passed

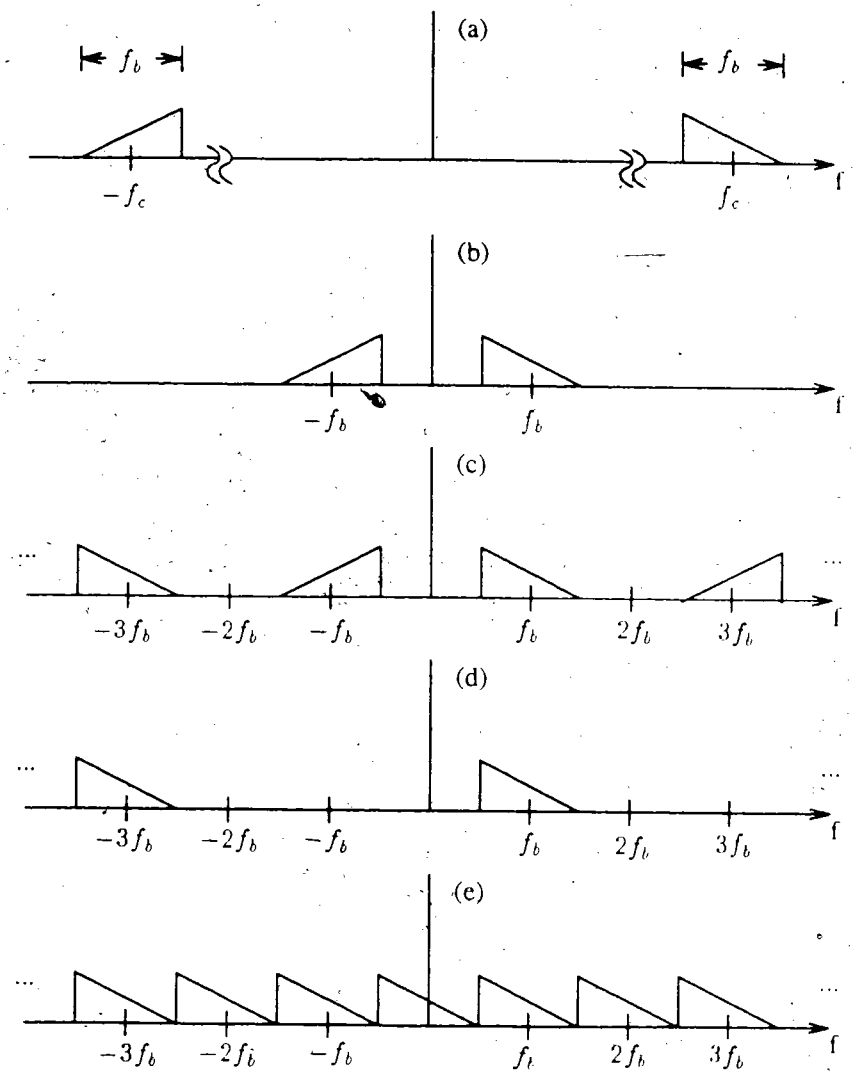

Figure 3.3: Spectrum of Hilbert transform demodulation process: (a) Spectrum of bandpass signal $x(t)$. (b) Spectrum of the down converted signal. (c) Spectrum of sampled IF signal. (d) Spectrum of the single sideband signal. (e) Spectrum of the baseband complex envelope.

through a Hilbert transformer and a delay block resulting in the single sideband signal Figure 3.3(d). The delay block is to account for the group delay of the Hilbert transform. The final step is to multiply the samples by $e^{-j\omega_b nT_s}$ to shift the spectrum so that the spectral image centred at f_b is moved to $f = 0$. This multiplication can be simplified since the sampling frequency is $4f_b$,

$$e^{-j\omega_b nT_s} = e^{-j2\pi f_b n/(4f_b)} \tag{3.1}$$

$$= e^{-j\pi n/2} \tag{3.2}$$

$$= \{1, j, -1, -j, 1, \cdots\} \tag{3.3}$$

By downsampling by four the output of both the Hilbert transform and the delay block, the samples are effectively multiplied by $e^{-j\omega_b nT_s}$, Figure 3.3(e), which results in samples of the complex envelope.

The impulse response of the Hilbert transform is [18]

$$h_H(n) = \frac{2\sin^2(\pi n/2)}{\pi n} \quad \text{n=integer} \tag{3.4}$$

The problem with this method is implementing $h_H(n)$ [18, 22, 24]. A practical implementation of the Hilbert transform departs from unity gain across the band resulting in a gain difference between the inphase and quadrature channels. The gain difference will result in a phase error of the demodulated complex envelope [24].

Another approach uses two bandpass filters with identical amplitude responses but 90° shifted in phase [21, 24, 25]. A block diagram showing the implementation of the 90° phase splitting method is shown in Figure 3.4. The demodulator's operation is similar to that of the Hilbert transform demodulator. The filter $H(\omega)$ removes the negative frequency sideband while leaving the positive frequencies alone. This requires the filter's response to be complex which is implemented using two real response filters

$$H(\omega) = H_1(\omega) + jH_2(\omega) \tag{3.5}$$

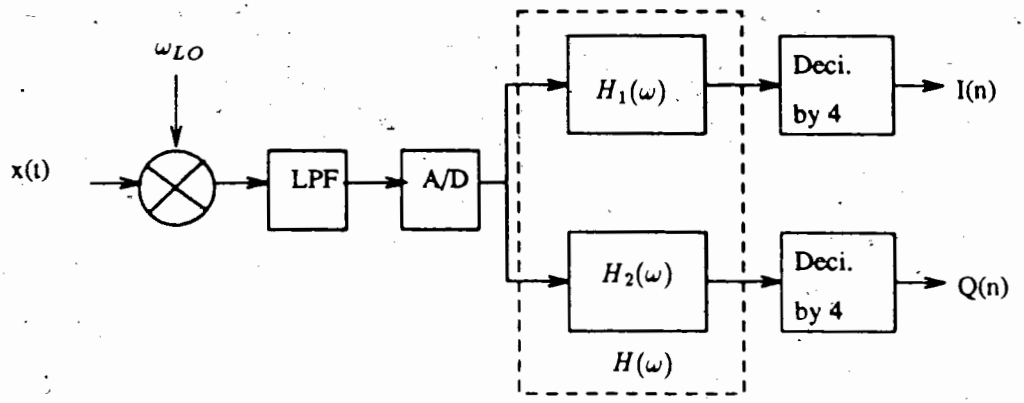

Figure 3.4: A quadrature demodulator that uses a 90° phase splitter.

The requirements for $H_1(\omega)$ and $H_2(\omega)$ are [21]

$$\begin{aligned} \angle H_2(\omega) - \angle H_1(\omega) &= \frac{\pi}{2} \quad -3\frac{\pi}{4} < \omega < -\frac{\pi}{4} \\ &= -\frac{\pi}{2} \quad \frac{\pi}{4} < \omega < 3\frac{\pi}{4} \end{aligned} \tag{3.6}$$

where ω is the normalized frequency. Both filters are all pass filters. The signal's frequency band must be contained within $\frac{\pi}{4} < \omega < 3\frac{\pi}{4}$. Both IIR and FIR implementations of filters that meet equation (3.6) are described in [21] and [24, 25] respectively.

3.2 Quadrature Demodulator

As described in section 2.1.2, when the beamforming process is performed on the complex envelope, the beamformer must delay the quadrature components. The previous techniques for recovering the complex envelope are not easily modified to realize the delayed quadrature components. A simple technique for quadrature demodulating a bandpass signal will now be described. This demodulator uses bandpass sampling to obtain samples of the I and Q channels and then employs interpolation to time register the samples. The same interpolation technique is used by the beamformer,

described in chapter 4, to delay the quadrature components, hence only a simple modification to the demodulator is required for beamforming.

3.2.1 Bandpass Sampling

If the aperture time of the A/D converter is small enough to avoid aperture errors, it is possible to recover the complex envelope from a bandpass signal by subsampling the signal and thereby eliminate any mixers [17, 22, 26]. Bandpass sampling also reduces the normally required sampling rate dictated by the Nyquist criteria, therefore the A/D requirements are relaxed. By properly choosing the sampling frequency, the periodic property of the Fourier transform of the sampling signal is exploited so that the bandpass signal is down converted to its complex envelope with little computational effort. Equations will now be derived for calculating the sampling frequency.

Using the equation describing a bandpass signal, equation (2.15), the I channel is sampled by sampling the bandpass signal when $\sin(\omega_c t) = 0$ and the Q channel is sampled when $\cos(\omega_c t) = 0$. For uniform sampling, the resulting samples of the bandpass signal are

$$\{I, Q, -I, -Q, I \cdots\} \tag{3.7}$$

if the sampling rate is

$$f_s = \frac{4f_c}{4n+3} \quad \text{n=0, 1, 2, } \cdots \tag{3.8}$$

and the samples are

$$\{I, -Q, -I, Q, I \cdots\} \tag{3.9}$$

if the sampling rate is

$$f_s = \frac{4f_c}{4n+1} \quad \text{n=0, 1, 2, } \cdots \tag{3.10}$$

These equations are derived by observing the carrier signal $\cos(\omega_c t)$ and $-\sin(\omega_c t)$, shown in Figure 3.5, along with the sampling intervals associated with equations (3.8)

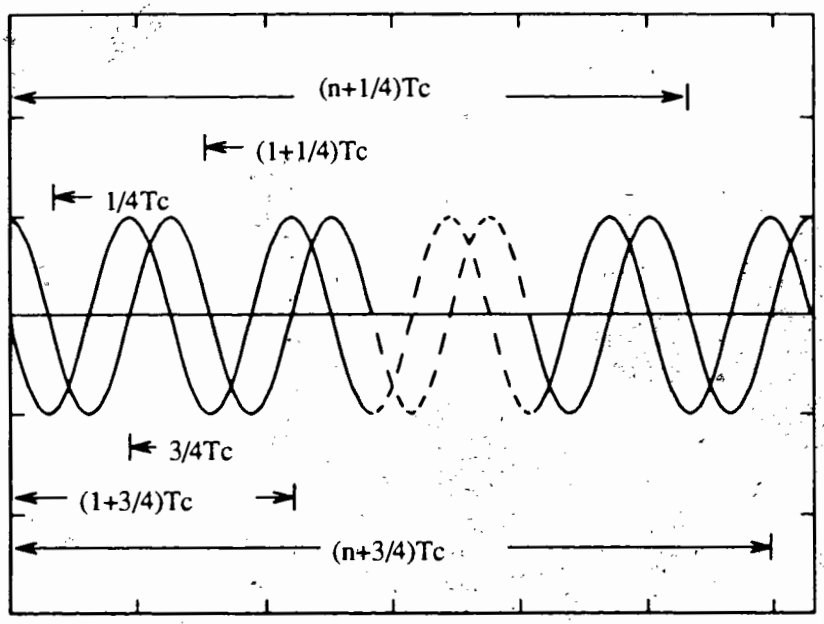

Figure 3.5: Illustration of the sampling points resulting in I and Q samples. The points shown at the bottom of the figure refer to equation (3.8) and the points at the top refer to equation (3.10). Tc refers to the carrier period.

and (3.10). For example, if the current sample is $+I$, (i.e., $\cos(\omega_c t) = 1$), the next sample is $+Q$ if $-\sin(\omega_c t + T_s) = 1$. The sampling period must then be $(n + 3/4)T_c$, where T_c is the carrier period, as shown at the bottom of Figure 3.5. If the sampling period is $(n + 3/4)T_c$, the sample following $+Q$ is $-I$ and then a $-Q$ followed by a $+I$ sample again. The sampling frequency is the reciprocal of the period which corresponds to equation (3.8). The same technique is used to derive equation (3.10) except now the sample following $+I$ must be $-Q$ so $-\sin(\omega_c t + T_s)$ must be equal to -1 and hence the sampling period is $(n + 1/4)T_c$.

Examining bandpass sampling in the frequency domain, Figures 3.6 and 3.7, illustrates the technique from a different perspective.

Figure 3.6(a) shows the spectrum of a bandpass signal, $x(t)$, whose bandwidth, f_b, includes any required guardband. For the bandpass spectrum to repeat itself in the region $0 < \omega < \pi$, an impulse is required in the sampling spectrum at either the highest frequency of the bandpass signal, f_h, or the lowest frequency of the bandpass signal, f_l.

For the sampling spectrum to have an impulse at f_h, then f_h must be an integer multiple of the sampling frequency, Figure 3.6(b)

$$f_h = kf_s \quad k = 1, 2, 3, \cdots \tag{3.11}$$

Substituting

$$f_h = f_c + \frac{1}{2}f_b \tag{3.12}$$

into (3.11) produces

$$f_c + \frac{1}{2}f_b = kf_s \tag{3.13}$$

The requirement of f_s to avoid aliasing of the complex envelope is

$$f_s = 2f_b \tag{3.14}$$

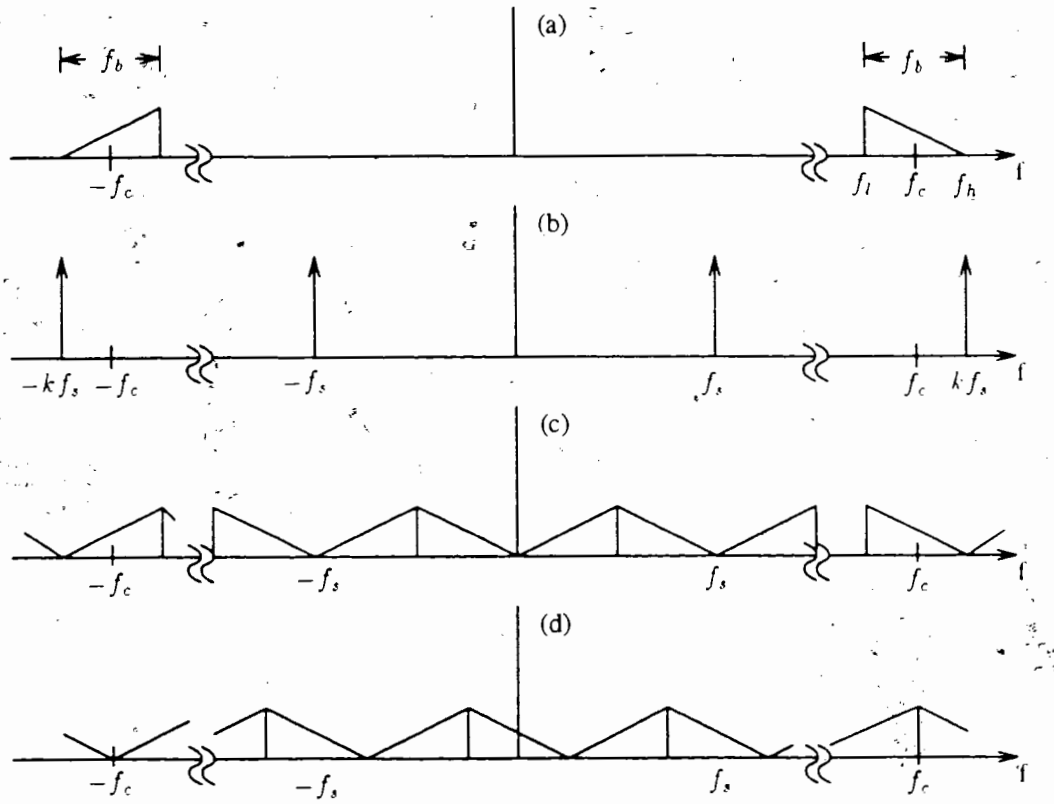

Figure 3.6: Spectrum of bandpass sampling process: (a) Spectrum of bandpass signal. (b) Spectrum of sampling signal. (c) Spectrum of sampled bandpass signal. (d) Spectrum of sampled signal shifted up in frequency.

Replacing f_b in (3.13) and solving for f_s results in the equation for the sampling frequency

$$f_s = \frac{4f_c}{4k-1} \tag{3.15}$$

Exchanging $n+1$ for k produces the following equation for the valid sampling frequencies

$$f_s = \frac{4f_c}{4n+3} \qquad n = 0, 1, 2, 3, \cdots \tag{3.16}$$

which is equivalent to equation (3.8).

The sampled-signal's spectrum, Figure 3.6(c), is the convolution of the bandpass signal spectrum and the sampling signal spectrum.

To centre the spectrum in Figure 3.6(c), it must be shifted up in frequency by $f_s/4$. This is accomplished by multiplying the signal by

$$e^{j2\pi f_s n T_s/4} = e^{j2\pi f_s n/(4f_s)} \tag{3.17}$$

$$= e^{j\pi n/2} \tag{3.18}$$

$$= \{1, j, -1, -j, 1, \cdots\} \tag{3.19}$$

Multiplying the sampled signal sequence in (3.7) by (3.19) results in the desired samples of the complex envelope.

$$\{I, jQ, I, jQ, \cdots\} \tag{3.20}$$

If an impulse is at f_l in the sampling-signal's spectrum, Figure 3.7(b), then

$$f_l = kf_s \quad k = 1, 2, 3, \cdots \tag{3.21}$$

Using the relationship

$$f_l = f_c - \frac{1}{2}f_b \tag{3.22}$$

equation (3.21) becomes

$$f_c - \frac{1}{2}f_b = kf_s \tag{3.23}$$

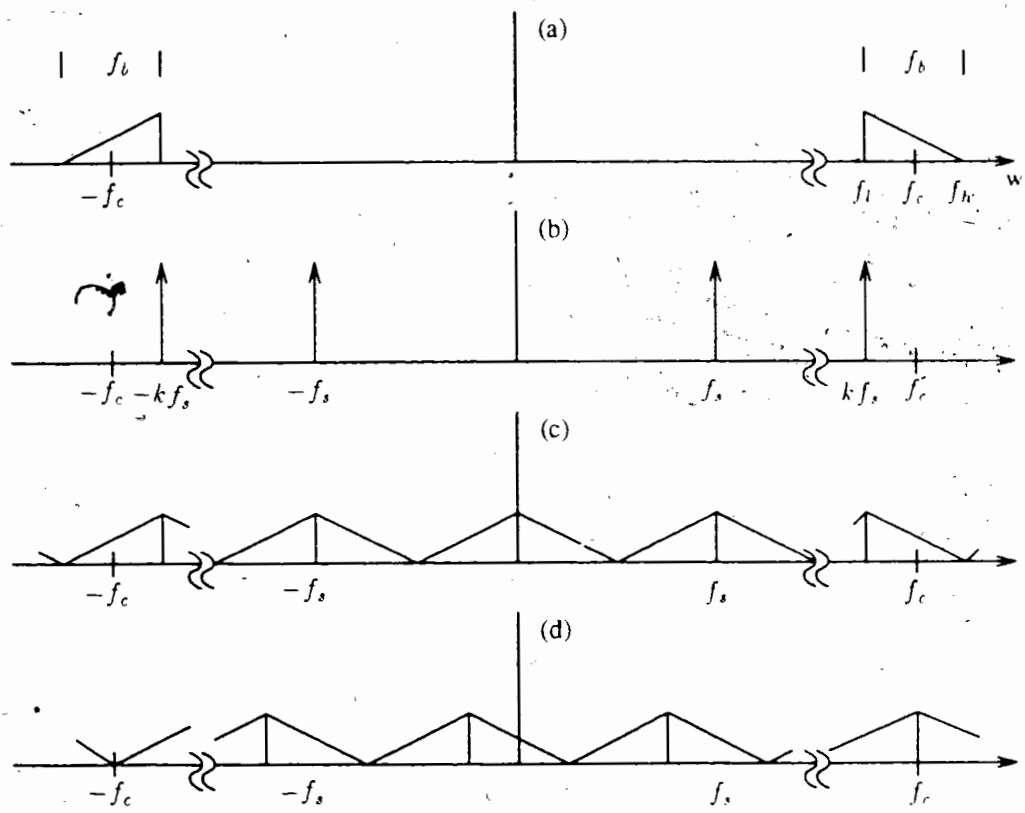

Figure 3.7: Spectrum of bandpass sampling process: (a) Spectrum of bandpass signal. (b) Spectrum of sampling signal. (c) Spectrum of sampled bandpass signal. (d) Spectrum of sampled signal shifted down in frequency.

Again, to avoid aliasing, the requirement of f_s is

$$f_s = 2f_b \tag{3.24}$$

Substituting equation (3.24) into equation (3.23) results in a second equation for valid sampling frequencies

$$f_s = \frac{4f_c}{4k+1} \tag{3.25}$$

which is equivalent to equation (3.10).

The subsampled-signal spectrum, Figure 3.7(c), is the convolution of the bandpass-signal spectrum and the spectrum of the sampling signal.

The final step is to centre the spectrum by shifting it down in frequency by $f_s/4$ and is carried out by multiplying the sampled signal by

$$e^{-j2\pi f_s n T_s/4} = e^{-j\pi n/2} \tag{3.26}$$

$$= \{1, -j, -1, j, 1, \cdots\} \tag{3.27}$$

This time, when the sampled sequence in (3.9) is multiplied by (3.27), the desired samples of the complex envelope is obtained.

The criteria that the sampling frequency be twice the bandpass bandwidth to avoid aliasing is evident in Figures 3.6 and 3.7. If it was not twice the bandpass bandwidth, there would be overlap of the individual spectrum in the sampled signal spectrum.

3.2.2 Interpolation

So far, a method has been described for recovering the complex envelope by bandpass sampling the signal. The obvious problem is that the I and Q samples are not both available at the same time. Interpolation is used to time register the samples by

estimating the value of I and the value of Q at a common reference time using the past and future samples of I and Q.

Figure 3.8 illustrates a number of samples of the inphase and quadrature signals

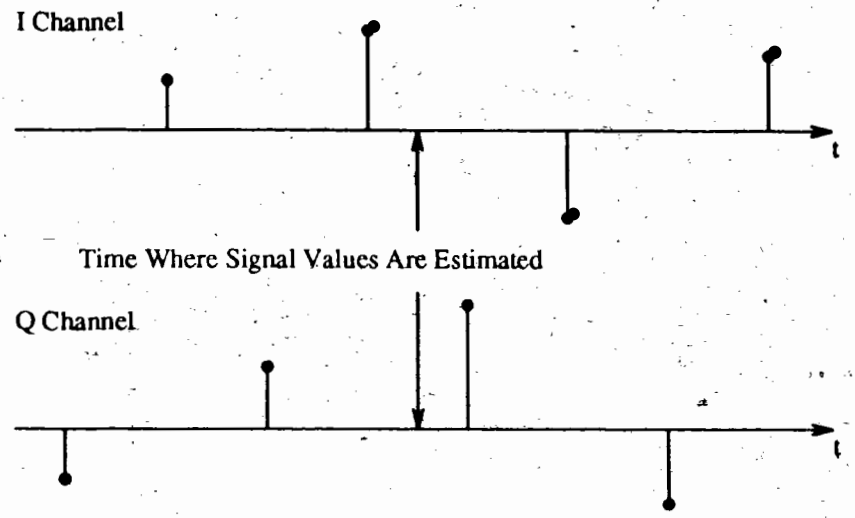

Figure 3.8: Interpolation point to time register the I and Q samples.

after the sign changes have been made. To time register the samples, one could leave the I channel as is and interpolate the Q channel to align it with I in time. This means the interpolated time shift is one sample time of the bandpass signal or 1/2 the sample time of the Q channel. Since the largest interpolation error occurs at 1/2 the sample time of the baseband signal and in the interest of symmetry, the I channel is interpolated forwards 1/4 sample and the Q sample is interpolated backwards 1/4 sample. These 1/4 samples refer to the baseband sampling rate and consequently, in terms of the bandpass sample rates, the time registry point is moved forwards 1/2 of a sample for the I channel and backwards 1/2 of a sample for the Q channel. Interpolating both channels spreads a smaller interpolation error over both channels.

Previous Interpolation Techniques

Interpolation can be used to effect a higher sampling rate [12, 14, 15]. The upsampling of a sequence can be viewed as a two step process, Figure 3.9. A signal is first sampled

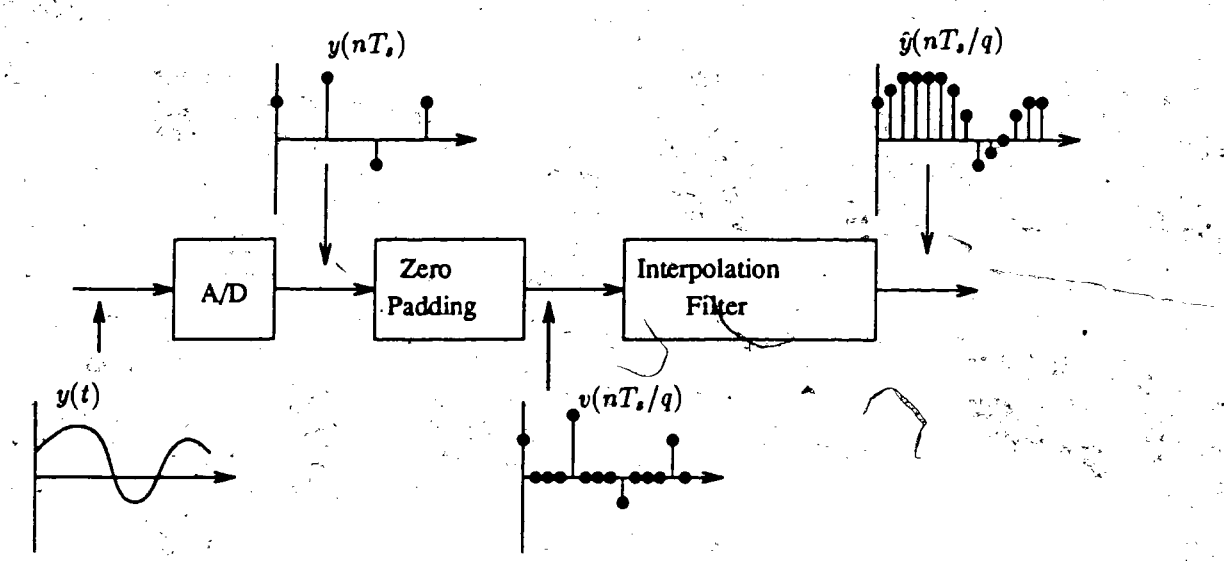

Figure 3.9: Block diagram showing the upsampling procedure.

at a rate of T_s to form the samples $y(nT_s)$. The sampled sequence is then padded with zeros between the data points. The zero-padded sequence, $v(nT_s/q)$, is then smoothed using a digital filter to produce $\hat{y}(nT_s/q)$, which is an estimate of $y(t)$ sampled at a rate of nT_s/q. The upsampling has effectively created a series of vernier delays which are used to estimate $y(t)$ between sample points. The appropriately interpolated sample is selected from the upsampled signal.

Figure 3.10 illustrates the interpolation process in the frequency domain which clearly indicates the interpolation filter requirements. The initial baseband-signal's spectrum, $Y(\omega)$, is shown in Figure 3.10(a). The spectrum of the sampled signal, $y(nT_s)$, is shown in Figure 3.10(b) and the zero-padded sequence, $v(nT_s/q)$, is shown in Figure 3.10(c). The purpose of the interpolation filter is to suppress the interme-

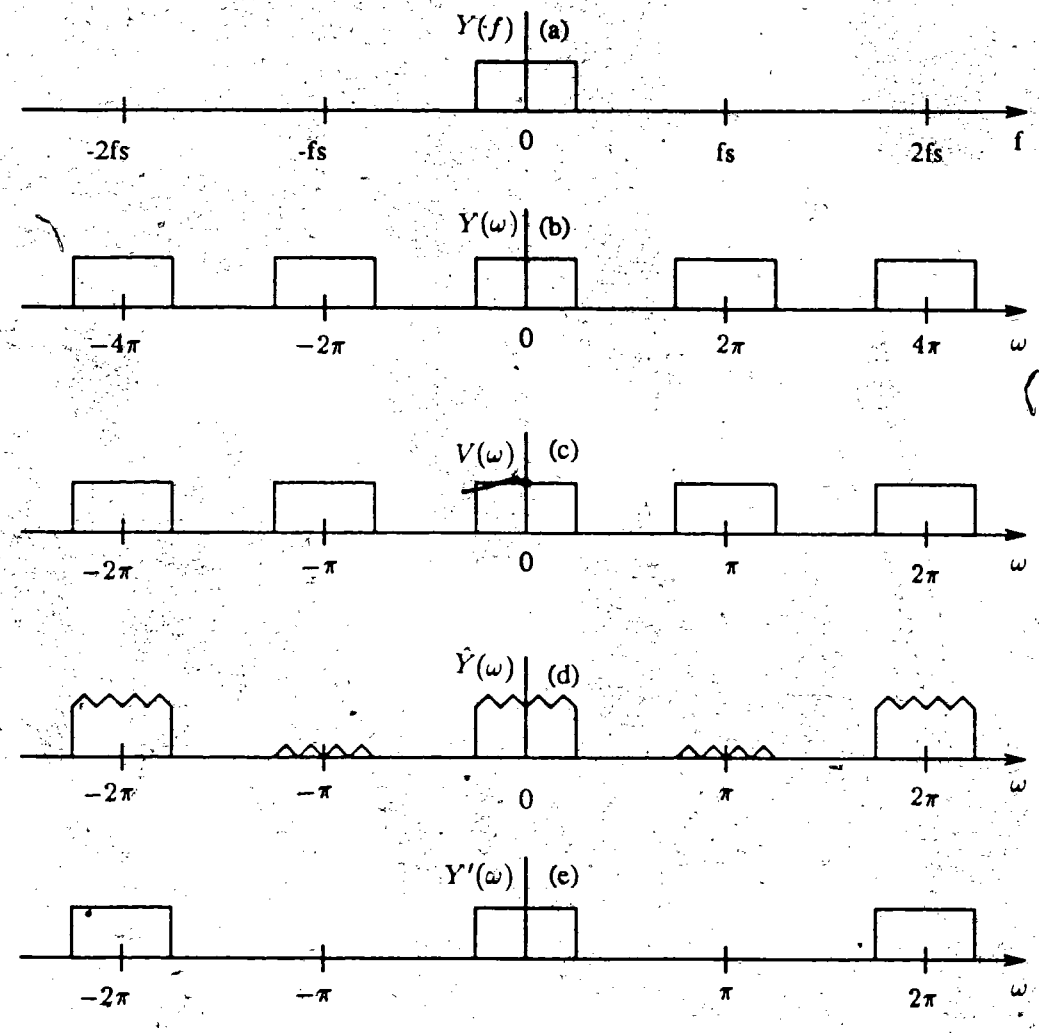

Figure 3.10: Spectra of the upsampling process for $q = 2$. (a) Spectrum of original signal. (b) Spectrum of the sampled signal. (c) Spectrum of the zero padded signal. (d) Spectrum of the filtered signal. (e) Spectrum of the desired signal.

diate spectra of $v(nT_s/q)$ so that the spectrum of $\hat{y}(nT_s/q)$ is approximately that of $y(nT_s/q)$. Figure 3.10(d) is the spectrum of $\hat{y}(nT_s/q)$ and Figure 3.10(e) is the spectrum of $y(nT_s/q)$. The two spectra differ due to nonideal filter characteristics such as passband ripple and a finite stopband. The nonideal characteristics contribute to the interpolation error and are controlled by increasing the filter complexity. Schafer

and Rabiner [15] used a 29 tap FIR filter to achieve a passband with 0.1 dB ripple and a stopband 45 dB down. The original signal was required to be sampled by at least three times its highest frequency and the filter was used to upsample the signal by six (i.e., provide five interpolated points between samples). The interpolation method used by our beamformer provides better interpolation performance with smaller filters.

One problem with the upsampling interpolation method is the difficulty of calculating the filter coefficients. For a desired interpolation point, a value for q needs to be found such that $v(nT_s/q)$ has a sample at the desired point. A second requirement of q is that it must divide the original sampling period evenly, i.e., q must be a integer. Normally, the signal is upsampled, and the interpolated signal closest to the desired point is used.

Methods have been developed to design interpolation filters whose coefficients are chosen to interpolate the signal at a desired point in time. If the highest frequency, f_{bh}, of a baseband signal is less than the half the sampling frequency, f_s, then the signal may be exactly reconstructed using [23]

$$y(t) = \sum_n y(n/f_s)s(t - n/f_s) \tag{3.28}$$

where

$$s(t) = \frac{\sin(\pi f_s t)}{(\pi f_s t)} \tag{3.29}$$

is the cardinal function. In practice, the summation in (3.28) is restricted to a finite sum. Specifically, equation (3.28) involves the summation of $2l + 1$ terms which provide an estimate, $\hat{y}(t)$, of $y(t)$ and the interpolation is realized using a FIR filter with coefficients calculated using (3.29).

An improvement in the interpolation error was found by replacing the cardinal function, equation (3.29), by [23]

$$s(t) = \left(\frac{\sin(\pi f_s tq/p)}{(\pi f_s tq/p)}\right)^p \frac{\sin(\pi f_s t)}{(\pi f_s t)} \tag{3.30}$$

where $q = 1 - 4f_{bh}/f_s$ and $p = Int(lq\pi/e)$. The symbol e is the base of the natural logarithm.

Figure 3.11 shows the mean squared error for interpolating a sinusoid when the

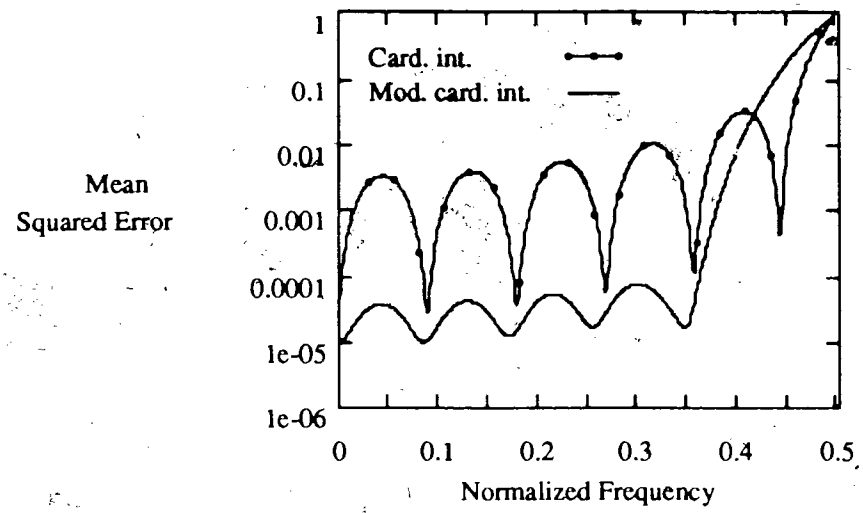

Figure 3.11: Error for interpolating a sinusoid, that has a nominal power of 1, using the cardinal function and the modified cardinal function. ($l = 5$)

FIR filter coefficients are calculated using equations (3.29) and (3.30). The interpolation filters each were of length eleven and the sampling frequency was four times the baseband bandwidth. The improvement in the error using equation (3.30) to calculate the filter coefficients is obvious.

Least Mean Squared Interpolation

The interpolation method in our beamformer employs an FIR filter whose coefficients depend on the point in time for the estimate. The criteria for calculating the FIR filter coefficients is to minimize the mean squared error between the actual value and the interpolated value.

The following derivation of the filter coefficients for interpolating between samples is similar to that found in [16] but modified for a single time point. The solution is in the form of the familiar normal equations so the development is presented in only enough detail to establish the notation and structures of the vectors and matrices. Let the sample sequence to be interpolated be represented by samples of $y(t)$ at $t = \pm 0.5$, ± 1.5, ± 2.5, $\cdots$ as shown in Figure 3.12 (this representation was chosen because it results in symmetric notation). The point to be interpolated lies between $y(-0.5)$

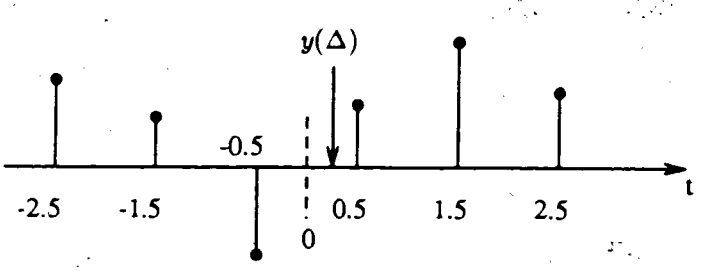

Figure 3.12: Interpolation of $y(\Delta)$.

and $y(0.5)$ and is denoted as $y(\Delta)$ where $-0.5 < \Delta < 0.5$. The estimate of $y(\Delta)$ is to be determined from k samples on either side. Let $\mathbf{y}$ be the vector containing $2k$ samples of the signal $y(t)$ and $\mathbf{b}$ be a vector containing the FIR filter coefficients. For the above example

$$\mathbf{y} = [y(-2.5), y(-1.5), y(-0.5), y(0.5), y(1.5), y(2.5)]^T \tag{3.31}$$

where ^{T} denotes matrix transposition. The interpolated value for $y(\Delta)$ is

$$\hat{y}(\Delta) = \mathbf{b}^T\mathbf{y} \tag{3.32}$$

The mean-squared error between the interpolated value, $\hat{y}(\Delta)$, and the actual value, $y(\Delta)$, is

$$\epsilon^2 = \mathrm{E}[(y(\Delta) - \hat{y}(\Delta))^2] \tag{3.33}$$

$$\epsilon^2 = \mathrm{E}[(y(\Delta) - \mathbf{b}^T\mathbf{y})^2] \tag{3.34}$$

$$\epsilon^2 = \mathrm{E}[y(\Delta)^2] - 2\mathbf{b}^T\mathrm{E}[y(\Delta)\mathbf{y}] + \mathbf{b}^T\mathrm{E}[\mathbf{y}\mathbf{y}^t]\mathbf{b} \tag{3.35}$$

Taking the gradient of ϵ^2 with respect to $\mathbf{b}$ and setting it to zero results in the following optimal solution for minimizing ϵ^2 [27]

$$\mathbf{b} = (\mathrm{E}[\mathbf{y}\mathbf{y}^T])^{-1}\mathrm{E}[y(\Delta)\mathbf{y}] \tag{3.36}$$

For general k we have

$$\mathrm{E}[y(\Delta)\mathbf{y}] = \mathbf{r}_y = \begin{bmatrix} \mathcal{R}_y(\Delta + (k-1) + 0.5) \\ \mathcal{R}_y(\Delta + (k-2) + 0.5) \\ \vdots \\ \mathcal{R}_y(\Delta + 0.5) \\ \mathcal{R}_y(\Delta - 0.5) \\ \vdots \\ \mathcal{R}_y(\Delta - (k-2) - 0.5) \\ \mathcal{R}_y(\Delta - (k-1) - 0.5) \end{bmatrix} \tag{3.37}$$

and

$$\mathrm{E}[\mathbf{y}\mathbf{y}^t] = \mathbf{R}_y = \begin{bmatrix} \mathcal{R}_y(0) & \mathcal{R}_y(-1) & \cdots & \mathcal{R}_y(-2k+1) \\ \mathcal{R}_y(1) & \mathcal{R}_y(0) & \cdots & \mathcal{R}_y(-2k+2) \\ \vdots & \vdots & \vdots & \vdots \\ \mathcal{R}_y(2k-1) & \mathcal{R}_y(2k-2) & \cdots & \mathcal{R}_y(0) \end{bmatrix} \tag{3.38}$$

where $\mathcal{R}_y(\tau)$ is the autocorrelation function of $y(t)$ defined as $\mathrm{E}[y(t+\tau)y(t)]$. Then, equation (3.36) becomes

$$\mathbf{b} = \mathbf{R}_y^{-1}\mathbf{r}_y \tag{3.39}$$

Equation (3.39) represents a generic solution to the interpolation problem when the sample period is normalized. In complex demodulation the inphase and quadrature baseband signals are interpolated separately. The samples used for interpolation are shown in Figure 3.8 where k is equal to 2, $\Delta = -0.25$ for the I channel and $\Delta = 0.25$ for the Q channel. The sample period is the baseband sample period normalized to 1 Hz.

Interpolation Error

There are two sources of error for this interpolation method. First the mean squared error, expressed in equation (3.35), is not zero and therefore we must ensure that it is negligible compared with other noise sources in the system, e.g., quantization noise. Second, the filter coefficients depend upon the autocorrelation function of the baseband signal. This is usually not known a priori or may change with time.

In considering the first source of error, $y(t)$ is assumed to be a band-limited white noise process as shown in Figure 3.13. The autocorrelation function, which is the

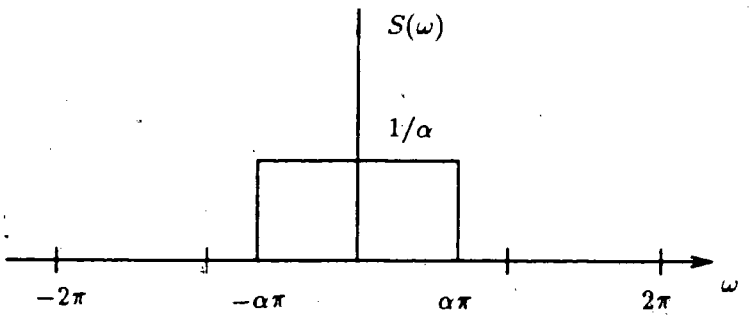

Figure 3.13: Power Spectral Density of a bandlimited white noise process.

inverse Fourier transform of the power spectral density, is

$$\mathcal{R}_y(\tau) = \frac{\sin(\alpha\pi\tau)}{\alpha\pi\tau} \tag{3.40}$$

Considering the interpolation error as noise, Figure 3.14 shows the resulting SNR for interpolating a band-limited white noise process for various values of Δ using a 10 tap filter (5 taps either side of the interpolation point) and $\alpha = 1/2$. Notice that the SNR depends on the distance between the nearest data sample and the sample point to be estimated and is lowest when the interpolation point is halfway between two data points, i.e. $\Delta = 0$.

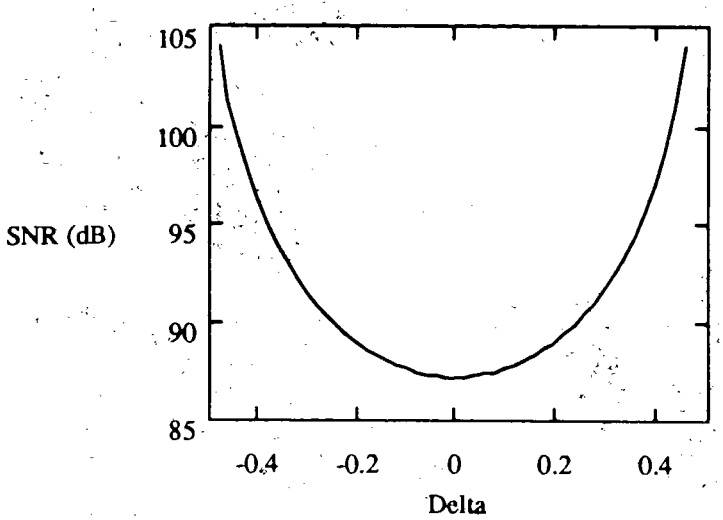

Figure 3.14: SNR of Optimum Interpolator for interpolating band limited white noise at various interpolation points. ($n = 10$, $\alpha = 1/2$)

The errors from the first source are made negligible by either increasing the sampling rate or increasing the length of the interpolation filters. Figure 3.15 illustrates the worst case SNR for various values of α. It is obvious that as the signal's bandwidth decreases, the SNR improves. Figure 3.16 shows how increasing the interpolation filter length improves the SNR. The tradeoff between baseband bandwidth and filter length is also evident. For example, if a SNR of 60dB is required, then a filter of length 12 would be necessary when $\alpha = 2/3$ (i.e., the baseband sampling rate is three times the bandwidth of the signal). However, if the sampling rate is increased to four times the bandwidth ($\alpha = 1/2$) then only an eight tap filter would be required, yielding an SNR close to 70dB.

Errors caused by a mismatch between the assumed autocorrelation function and the actual autocorrelation function of the signal are not as easily determined because in practice the autocorrelation function is not known. Since a white noise process contains all frequencies in its bandwidth, it is reasonable to expect, however, that

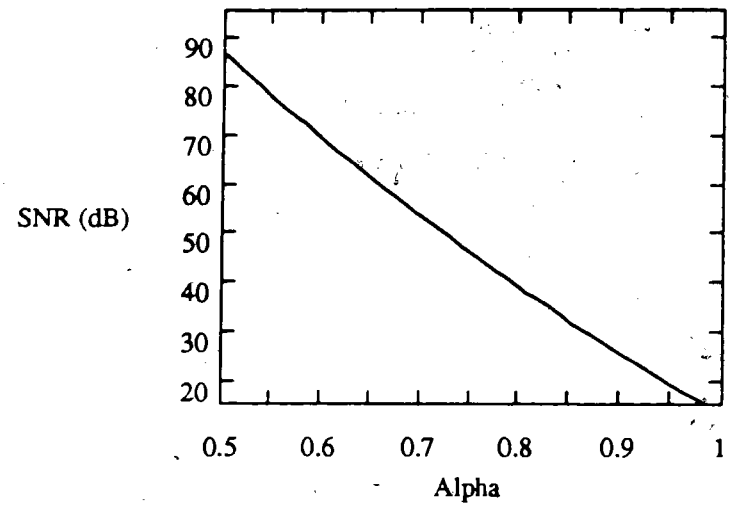

Figure 3.15: Worst case SNR of Optimum Interpolator for various values of α. ($n = 10$, $\Delta = 0$)

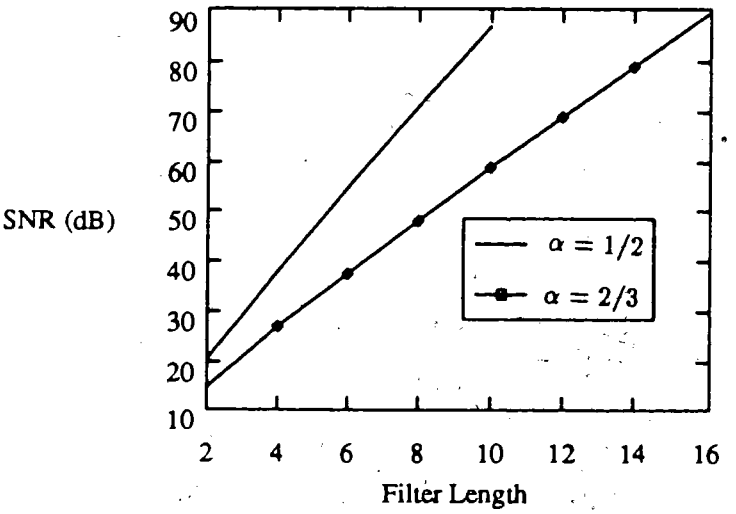

Figure 3.16: Worst case SNR of Optimum Interpolator for various filter lengths and bandwidths. ($\Delta = 0$)

an interpolation filter designed to handle band-limited white noise would perform well for any signal with an equal or smaller upper frequency limit. To verify this argument, a filter was designed to interpolate band-limited white noise. This filter's performance was tested by interpolating a sinusoidal signal of various frequencies and normalized power. The mean squared error was predicted using

$$\epsilon^2 = \mathrm{E}[(y(\Delta) - \hat{y}(\Delta))^2] \tag{3.41}$$

$$\epsilon^2 = \mathcal{R}_s(0) - 2\mathbf{b}^T\mathbf{r}_s + \mathbf{b}^T\mathbf{R}_s\mathbf{b} \tag{3.42}$$

where $\mathcal{R}_s(\tau)$ is the autocorrelation for a sinusoid of random phase and $\mathbf{r}_s$ and $\mathbf{R}_s$ are similar to equations (3.37) and (3.38) except $\mathcal{R}_s$ is used instead of $\mathcal{R}_y$. The autocorrelation for a sinusoid is [28]

$$\mathcal{R}_s(\tau) = \cos(\omega_c\tau) \tag{3.43}$$

The vector $\mathbf{b}$ is the set of optimal filter coefficients calculated using equation (3.39) assuming a band limited white noise process. This error was compared with that obtained by a simulation method whereby samples of a sinusoid were passed through a filter whose coefficients were calculated assuming a white noise signal. The squared error was calculated for 500 random phase sinusoids and then averaged.

The predicted results and the simulated results are shown in Figures 3.17 and 3.18 respectively. The normalized bandwidth was 1/4Hz, ($\alpha = 1/2$), and the number of taps was 10. The interpolation point was taken halfway between two samples to maximize the interpolation error, i.e., $\Delta = 0$. Both methods generated the same results for the interpolation error. The peak interpolation noise is approximately 82 dB down which agrees with the value shown in Figure 3.16 for $\alpha = 1/2$ and $n = 10$. Figure 3.19 shows the interpolation error on a larger scale and how the error increases rapidly for signals out of the assumed band.

These results demonstrate that interpolation filters designed to handle band-limited white noise can be expected to perform well on signals with equal or lower upper frequency limits.

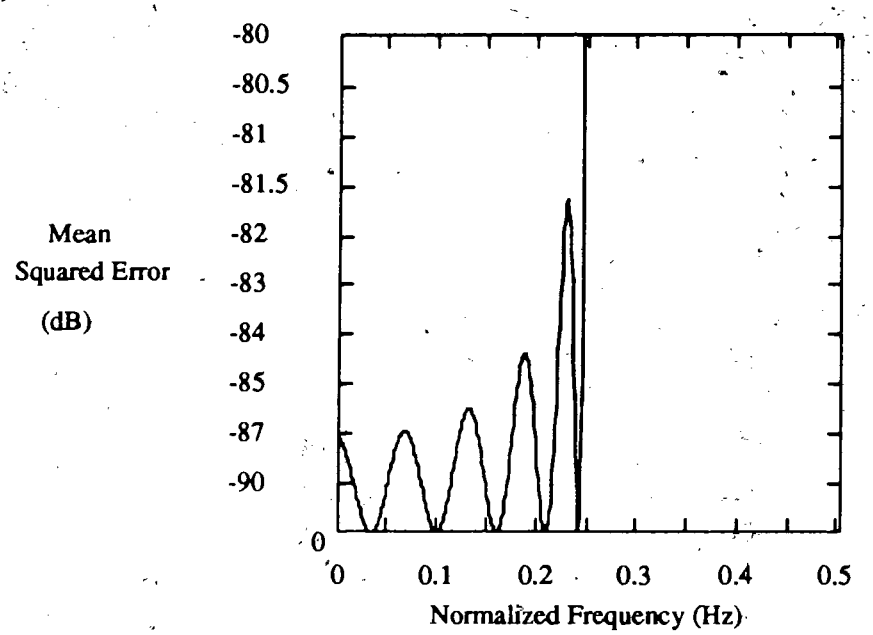

Figure 3.17: Predicted interpolation error for a sinusoid using least mean squared interpolation. ($\Delta = 0$, $n = 10$, $\alpha = 1/2$)

The interpolation error when the least mean squared method is used to compute the filter coefficients is compared to the error when the filter coefficients are calculated using the modified cardinal series in Figure 3.20. The least mean squared interpolation filter was of length ten and the modified cardinal series filter was of length eleven. Both errors are calculated by simulation methods. There is at least a 30 dB improvement using the least mean squared interpolation method over the modified cardinal series method.

3.2.3 Implementation of a Quadrature Demodulator

The quadrature demodulator uses the least mean square interpolation method to time register the I and Q samples. As evident in the sequences in (3.7) and (3.9),

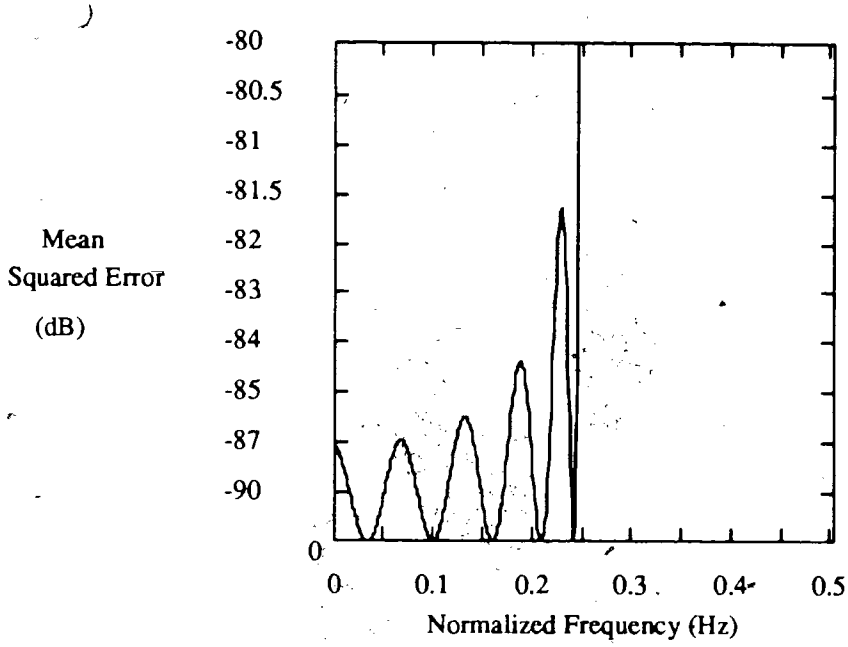

Figure 3.18: Simulated interpolation error for a sinusoid using least mean squared interpolation. ($\Delta = 0$, $n = 10$, $\alpha = 1/2$)

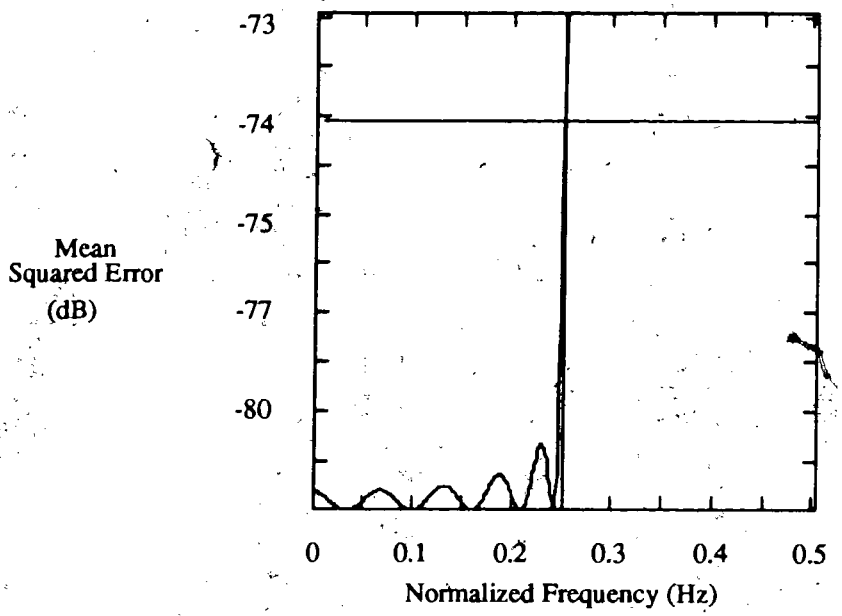

Figure 3.19: Interpolation error on expanded scale.

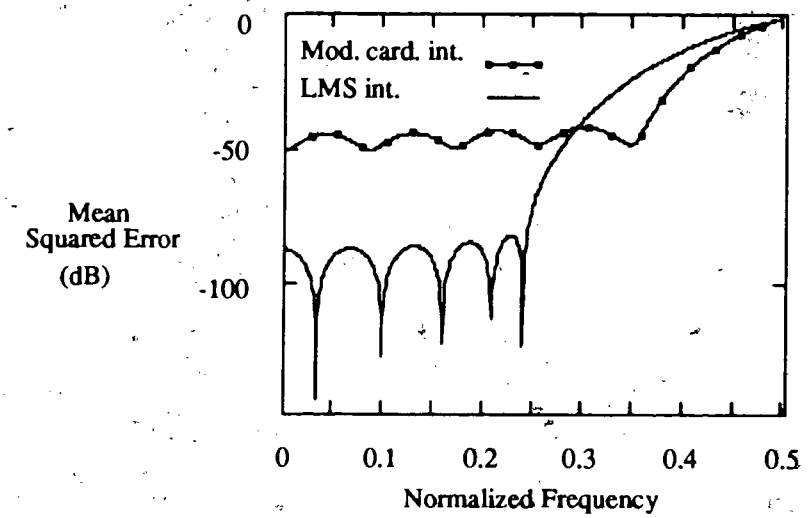

Figure 3.20: Comparison of interpolation error using both the least mean squared method (length 10) and the modified cardinal series (length 11).

every other sample of I and Q needs to be negated. However, if every second filter coefficient is inverted instead, then the samples can be passed directly through the filters, and either every second output sample from the filter is sign inverted or the filter output is decimated by 2. Either way, the sampling rate should be high enough so that the output rate is at least twice the highest frequency in the baseband signals to prevent aliasing. In the beamformer, sign changes are avoided by decimating the filter's output. A block diagram of a quadrature demodulator using the down sampling technique is shown in Figure 3.21. The A/D converter subsamples the

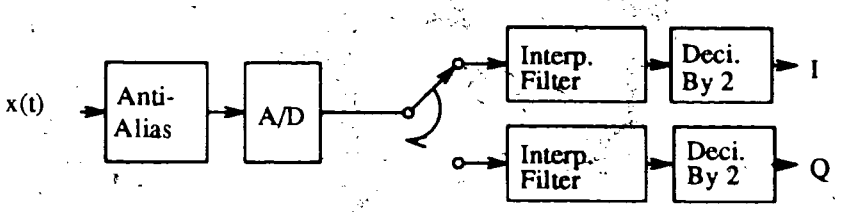

Figure 3.21: A quadrature demodulator block diagram.

bandpass signal, $x(t)$, to obtain samples of $I(t)$ and $Q(t)$ as explained in section 3.2.1. The samples from the A/D are then divided into data streams of just the I channel and just the Q channel. The two interpolation filters then time register the I and Q samples to a common point, shown in Figure 3.8. Every second filter coefficient is negated to account for every second I sample and Q sample being negated. Finally, the filter's output is decimated by 2 to avoid having to negate any of the samples.

In summary, the design methodology is:

- Decide on a noise level that will be negligible compared to the A/D quantization noise. For example, if using a 12 bit A/D converter (i.e., 72 dB dynamic range) an interpolation noise level 85 dB down will be negligible.
- Determine the bandpass sampling frequency using either equation (3.8) or (3.10). If decimating the output by 2, then the sampling frequency must be at least

four times the bandpass bandwidth (i.e., $\alpha = 1/2$) to prevent aliasing of the I and Q channels.

- Determine the interpolation filter length for $\alpha = 1/2$ and the noise is 85 dB down. Using Figure 3.16, a filter with 10 taps will meet the requirements.

Chapter 4

True Time Delay Bandpass Beamforming

It was shown in chapter 2 that to coherently combine the complex envelopes from a number of hydrophones, three distinct processes are required. First, the received bandpass signal must be down converted to its complex envelope representation. Second, the complex envelope must be delayed and finally rotated in phase. This chapter describes how the three process can be accomplished using the bandpass sampling and interpolation techniques described in chapter 3.

The first step, down converting the bandpass signal into its I_i and Q_i components by subsampling the signal, was explained in section 3.2.1. The subscript i identifies a particular hydrophone in the array. In brief, the bandpass signal is subsampled at a sampling frequency calculated using either equation (3.8) or equation (3.10). The resulting samples are alternating samples of $I_i(t)$ and $Q_i(t)$.

The next step is to time delay the quadrature components to obtain $I_i(nT_O - \tau_i)$ and $Q_i(nT_O - \tau_i)$. The required delay, τ_i, is divided into an integer number of sample periods and a fraction of a sample period. The integer number of periods to be

delayed is implemented by simply shifting the sequence of the I_i and Q_i samples in time. Interpolation, described in section 3.2.2, is then used to estimate I_i and Q_i at the fraction of the sample period. Estimates of $I_i(nT_O - \tau_i)$ and $Q_i(nT_O - \tau_i)$ are

$$I_i(nT_O - \tau_i) = \mathbf{a}_i^T \mathbf{I}_i \tag{4.1}$$

$$Q_i(nT_O - \tau_i) = \mathbf{b}_i^T \mathbf{Q}_i \tag{4.2}$$

where $\mathbf{I}_i$ and $\mathbf{Q}_i$ are vectors which contain the samples of $I_i(t)$ and $Q_i(t)$ respectively. Each vector contains an equal number of samples on either side of the point to be interpolated. The vectors $\mathbf{a}_i$ and $\mathbf{b}_i$ contain the optimum filter coefficients for interpolating $I_i(nT_O - \tau_i)$ and $Q_i(nT_O - \tau_i)$. Figure 4.1 illustrates the process of time shifting the quadrature components. The I and Q channels are shifted an integer number of sample periods and then interpolated to a fraction of a sample period. If no delay is required then $\tau_i = 0$, and the required operation is then to simply demodulate the bandpass signal into its quadrature components, and time register the samples as described in section 3.2.

The final step is to rotate the complex envelope in phase. The delayed quadrature components are multiplied by either $\cos(\omega_c \tau_i)$ or $\sin(\omega_c \tau_i)$ and then added together to obtain the complex envelope of the delayed bandpass signal, Figure 4.2.

It is possible to accomplish both the delay and the phase rotation using a single FIR filter per channel for each hydrophone. This avoids having to cross multiply the signals and divide the samples into I and Q samples and results in a simpler architecture. For example, the equation for $I_{Di}(nT_O)$, from equation (2.21), is

$$I_{Di}(nT_O) = \cos(\omega_c \tau_i) I_i(nT_O - \tau_i) + \sin(\omega_c \tau_i) Q_i(nT_O - \tau_i) \tag{4.3}$$

substituting equations (4.1) and (4.2) for $I_i(nT_O - \tau_i)$ and $Q_i(nT_O - \tau_i)$ yields

$$I_{Di}(nT_O) = \cos(\omega_c \tau_i) \mathbf{a}_i^T \mathbf{I}_i + \sin(\omega_c \tau_i) \mathbf{b}_i^T \mathbf{Q}_i \tag{4.4}$$

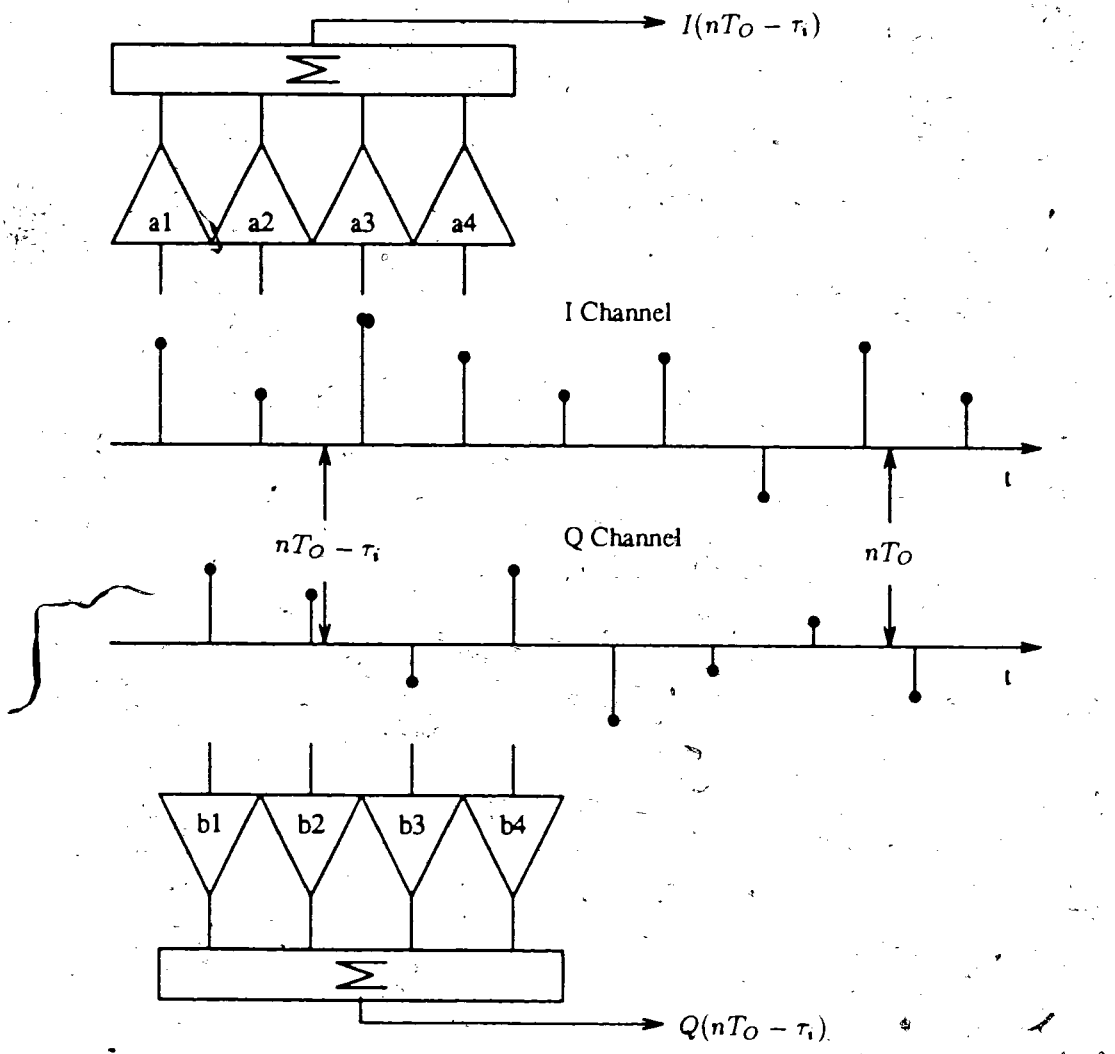

Figure 4.1: Time shifting the I channel and the Q channel to form $I_i(nT_O - \tau_i)$ *and* $Q_i(nT_O - \tau_i)$.

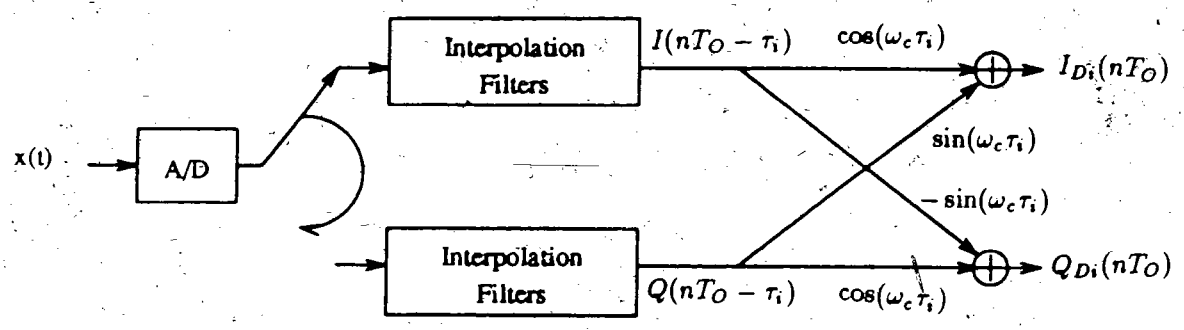

Figure 4.2: Cross multiplying the delayed quadrature components to form the quadrature components of the delayed bandpass signal.

Each of the filter coefficients, a_{in} and b_{in}, can be multiplied by $\cos(\omega_c \tau_i)$ and $\sin(\omega_c \tau_i)$ resulting in two new vectors $\mathbf{c}_i$ and $\mathbf{d}_i$. Substituting $\mathbf{c}_i$ and $\mathbf{d}_i$ into equation (4.4) results in

$$I_{Di}(nT_O) = \mathbf{c}_i^T \mathbf{I}_i + \mathbf{d}_i^T \mathbf{Q}_i \tag{4.5}$$

Since the samples in $\mathbf{I}_i$ and $\mathbf{Q}_i$ make up the samples of the bandpass signal, $x_i(t)$, rather than divide the data into $\mathbf{I}_i$ and $\mathbf{Q}_i$, the sampled bandpass signal can be passed directly through a new FIR filter whose coefficients are $\mathbf{c}_i$ merged with $\mathbf{d}_i$. That is

$$I_{Di}(nT_O) = \mathbf{v}_i^T \mathbf{x}_i \tag{4.6}$$

where

$$\mathbf{v}_i^T = [\cos(\omega_c \tau_i) a_{i1}, \sin(\omega_c \tau_i) b_{i1}, \cos(\omega_c \tau_i) a_{i2}, \cdots, \cos(\omega_c \tau_i) a_{iL}, \sin(\omega_c \tau_i) b_{iL}] \tag{4.7}$$

and $\mathbf{x}_i$ are the samples of the bandpass signal from hydrophone i.

A similar argument is used to derive the coefficients for a filter to generate Q_{Di}

$$Q_{Di}(nT_O) = -\sin(\omega_c \tau_i) \mathbf{a}_i^T \mathbf{I}_i + \cos(\omega_c \tau_i) \mathbf{b}_i^T \mathbf{Q}_i \tag{4.8}$$

$$Q_{Di}(nT_O) = \mathbf{f}_i^T \mathbf{I}_i + \mathbf{g}_i^T \mathbf{Q}_i \tag{4.9}$$

where

$$\mathbf{f}_i = -\sin(\omega_c \tau_i) \mathbf{a}_i \tag{4.10}$$

and

$$\mathbf{g}_i = \cos(\omega_c \tau_i)\mathbf{b}_i \tag{4.11}$$

Again, a new filter, whose coefficients are $\mathbf{w}_i$, can be obtained by merging $\mathbf{f}_i$ with $\mathbf{g}_i$. $Q_{Di}(nT_O)$ is then

$$Q_{Di}(nT_O) = \mathbf{w}_i^T \mathbf{x}_i \tag{4.12}$$

A complete mathematical explanation on how to calculate the filter coefficients $\mathbf{v}_i$ and $\mathbf{w}_i$ using matrix algebra is given in appendix A.

Therefore, by using two FIR filters per hydrophone, as shown in Figure 4.3, both the I_{Di} and Q_{Di} signals can be demodulated with the proper phase rotation and time delay. Even though these filters have twice as many taps, the resulting architecture is much simpler. The demodulated outputs from each receiver are then added together to generate the output from the beamformer as shown in the block diagram in Figure 4.4.

The decimation by 4 is required to avoid making sign changes. Until now, every other sample of I_i and Q_i was assumed to be negated so that the sampled bandpass signal was $\{I, Q, I, Q, \cdots\}$. Again, like the case for the demodulator, having to negate samples can be avoided by instead negating every second value of the filter coefficients a_{in} and b_{in}. The input sequence is then required to be shifted by four bandpass sample periods for every output sample to ensure that the samples are multiplied by the correct coefficients. To avoid aliasing, the sampling frequency must be large enough so that the output rate is at least twice the highest frequency in the quadrature signals which implies that the bandpass sampling frequency must be at least four times the bandpass bandwidth. This also ensures that the baseband sampling rate is high enough to provide good interpolation (i.e., $\alpha < 1/2$).

If several different beams are required simultaneously, then several beamformers can be used, each receiving the signals from the hydrophones in the array but

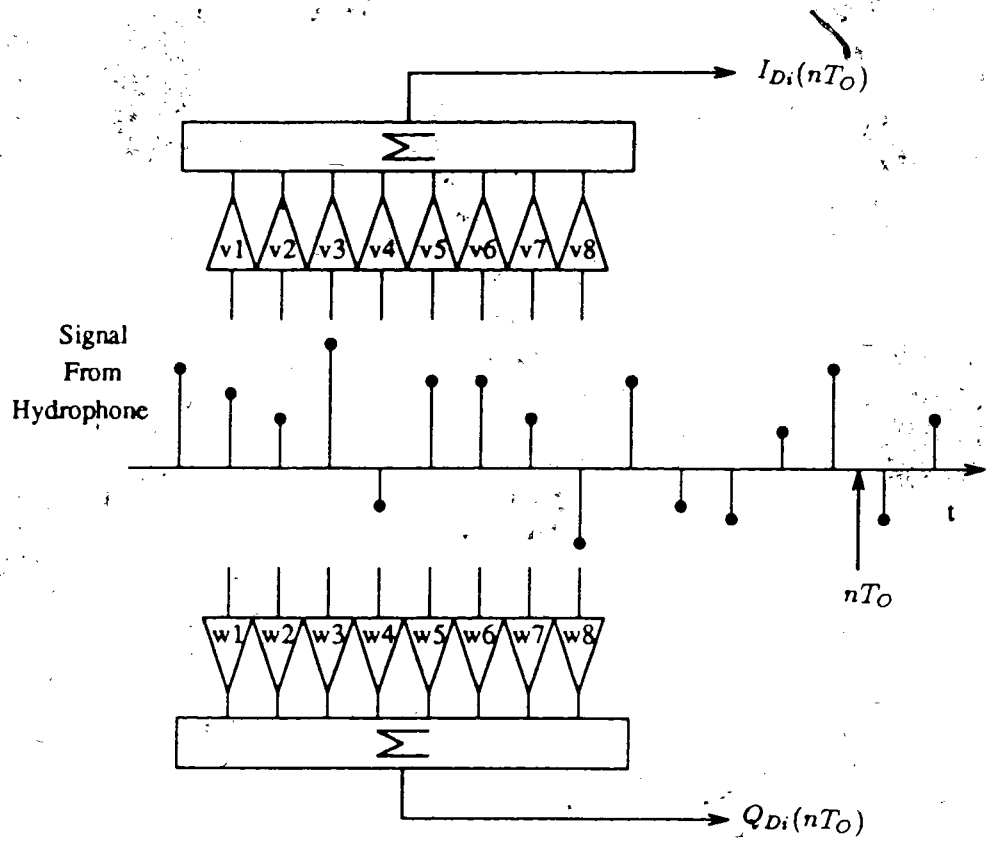

Figure 4.3: Delaying and phase rotating the quadrature components directly from the bandpass signal samples.

each having a different look direction. A block diagram of the multibeam configuration is shown in Figure 4.5. A possible implementation is that each beamformer is constructed on a separate card. Although this implementation may require more hardware than the FFT beamformer, it does have the advantage of:

Greater flexibility

-Only as many beams as required

-Arbitrary arrays

-Continuously steerably beams

Less complexity in the hardware

-Serial data streams and modularity

Soft Degradation

-If one fails, the rest will continue to operate

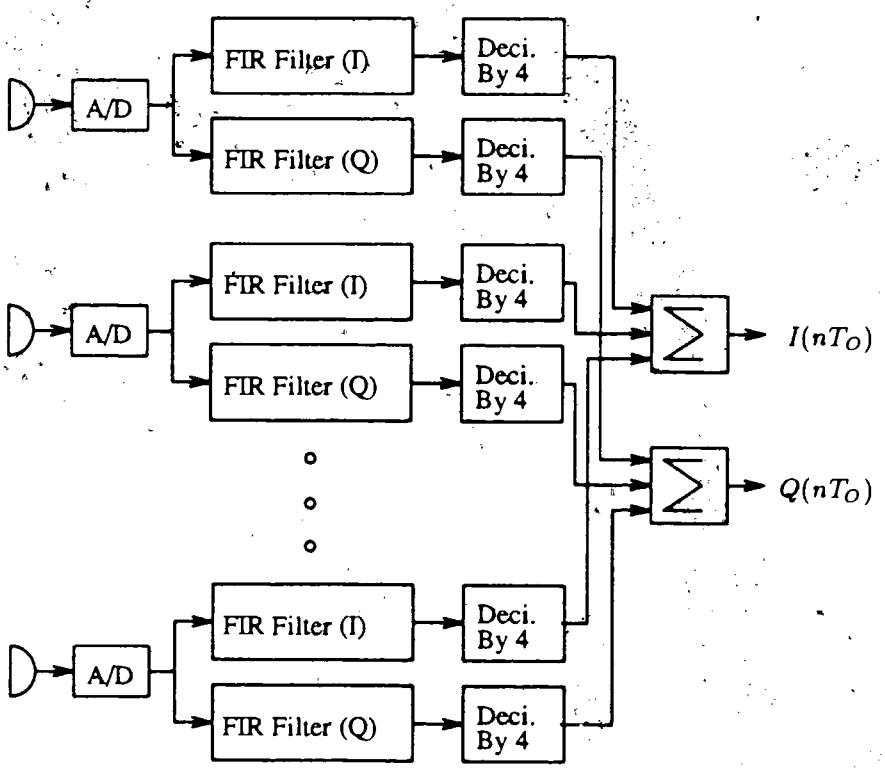

Figure 4.4: Block diagram of the True Time Delay Bandpass Beamformer.

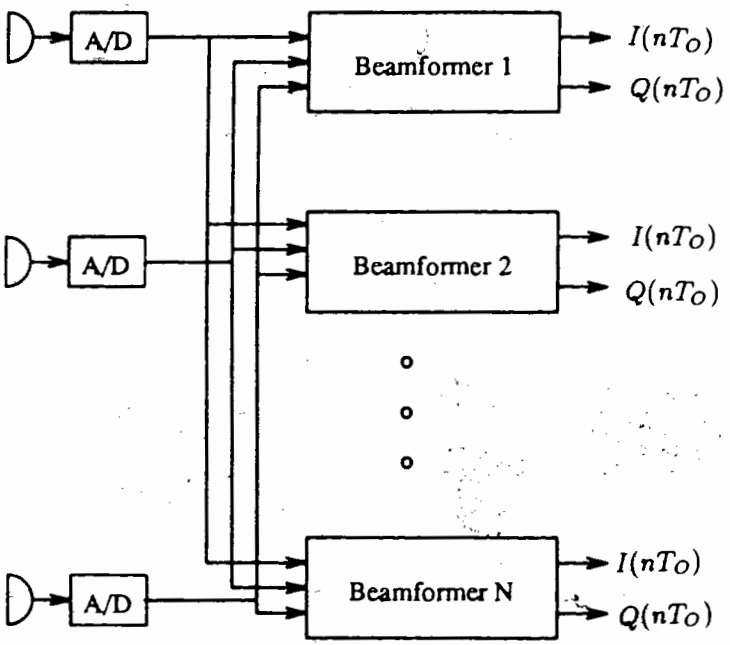

Figure 4.5: Block diagram of multiple beam beamformer.

Chapter 5

A Design Example and Results

5.1 The Underwater Testbed

The underwater acoustic testbed, developed by the Underwater Research Lab at Simon Fraser University, is a tool for studying the underwater acoustic channel. The testbed transmits a gated sinusoid signal and then receives and coherently demodulates the signal to complex baseband. The demodulation technique described in section 3.2 is used to recover the complex envelope. The testbed consists of a network of four computers (three 286 machines and a 386 machine), Figure 5.1. The 386 computer is the surface node and it both processes the received data and controls the testbed. The surface node is able to plot the sampled signal and the demodulated complex envelope, and generate the phase plot representing the complex envelope. One of the 286 machines acts as a file server for the network. The remaining two 286 machines are 'little board' computers and are ment to go below the surface in watertight containers. These two computers control the transmit and receive circuitry.

The transmit circuitry generates a gated sinusoid signal whose pulse length is

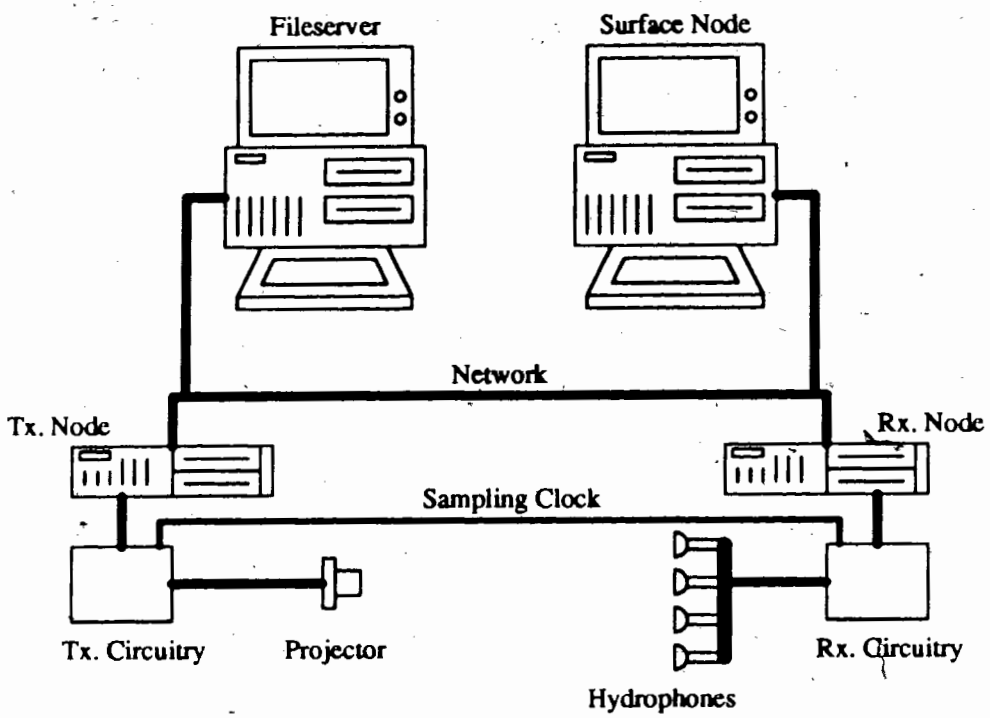

Figure 5.1: The Acoustic Testbed

controlled by the user. The signal is then amplified by a 120 W amplifier and sent to an acoustic projector. The transmitter also provides a sampling clock for the receiver that is synchronized with the carrier signal. The receiver uses the sampling clock to bandpass sample the received signals.

The receiver receives signals for up to four channels. The signals are first amplified and then filtered with a 4 kHz bandpass filter. The receiver then uses the sampling clock to bandpass sample the filtered signals, section 3.2.1, using a 12 bit analog to digital converter. The digitized signals are then transmitted to the control node, via the network, for processing.

5.2 Design Example and Test Environment

The proposed beamformer was implemented on a Sun Sparc station using Fortran 77. Given the location of the hydrophones in the array, and the look direction, the program first calculates the required filter coefficients for each of the hydrophones. It then passes hydrophone data, stored in files, through the filters to delay and phase rotate the complex envelope and finally it sums the filter outputs to generate the beamformer output.

The testbed was used to simultaneously sample the signal from each of the hydrophones in the array. The samples were then up-loaded onto the Sparc workstation to undergo the beamforming. The filters used in the beamformer were of length 20 (interpolation filters of length 10 time 2 for phase rotation) and the carrier frequency was 24 kHz. Interpolation filters of this length provide an interpolation SNR of 87 dB ($\alpha = 1/2$), Figure 3.15, which is better than the 72 dB SNR obtained with the 12 bit A/D converter [18]

There are a number of sampling frequencies that could be used to recover the complex envelope. The bandpass sampling frequencies that generate the $\{I, Q, -I, -Q, I, \cdots\}$ sequence, equation (3.8), are

$$32000 \text{ Hz}, 13714 \text{ Hz}, 8727 \text{ Hz}, 6400 \text{ Hz}, \cdots$$

and the sampling frequencies that generate the $\{I, -Q, -I, Q, I, \cdots\}$ sequence, equation (3.10), are

$$96000 \text{ Hz}, 19200 \text{ Hz}, 10667 \text{ Hz}, 7385 \text{ Hz}, \cdots$$

But, as was explained in chapter 4, the sampling frequency must be greater than four times the bandpass bandwidth. For this case, the bandpass bandwidth was 4 kHz so

the sampling frequency had to be larger than 16 kHz. The valid sampling frequencies are then

32000 Hz, 96000 Hz, 19200 Hz

A sampling frequency of 19.2 kHz was chosen.

Three trials were conducted to test the beamformer. All the trials were conducted on a barge owned by Simrad Mesotech Ltd. The barge was in about 12 m of water at Reed Point Marina in Burrard Inlet. An array consisting of three hydrophones spaced 3 cm apart, which is approximately $\frac{\lambda}{2}$ at the carrier frequency of 24 kHz, was used for the first two trials. The hydrophones were mounted on a jig designed to have a small profile to minimize any reflections that could cause interference [1]. The distance between the acoustic projector and the array was approximately 70 cm and both were submerged to a depth of 2 m. The gated pulse length was 2 ms long. For the third trial, two hydrophones were spaced approximately 1 m apart so that there was a considerable delay, relative to the pulse length, between the signal arriving at the hydrophones. The hydrophones were each mounted on a separate aluminum pole to hold them in position. The pulse length had to be reduced to 1.3 ms to prevent interference between the direct arrival and the surface reflection.

5.3 Trial Number 1

For the first trial, the incident angle of the signal onto the array was 0° (i.e., broadside) as shown in Figure 5.2. In such a situation, no time delay or phase rotation is required.

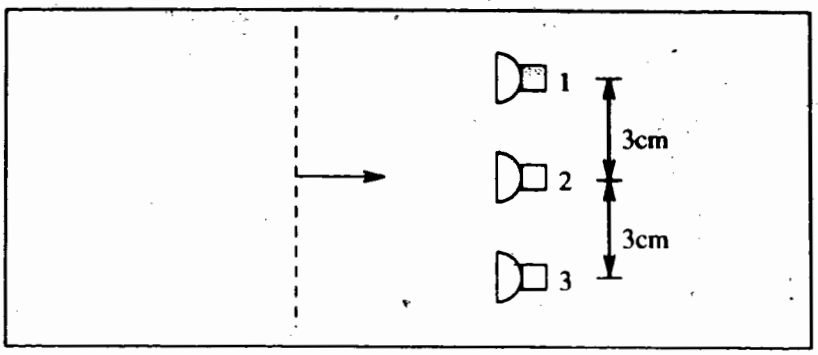

Figure 5.2: Hydrophone setup for the first trial.

The beamformer simply time registers the I and Q samples and then adds the complex envelopes together to form the beamformed output. Figure 5.3 shows the complex envelope from each of the hydrophones. The processed signal is shown in Figure 5.4 and is simply the sum of the complex envelopes of the hydrophone signals.

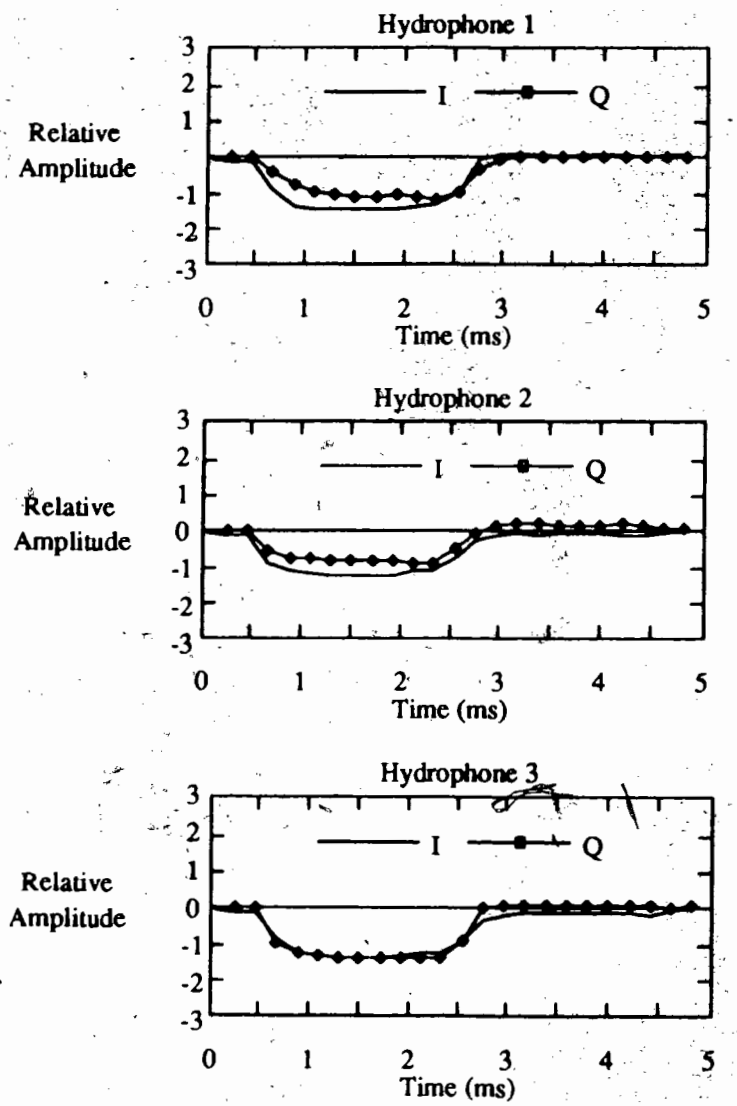

Figure 5.3: Demodulated signals from each of the hydrophones for the first trial.

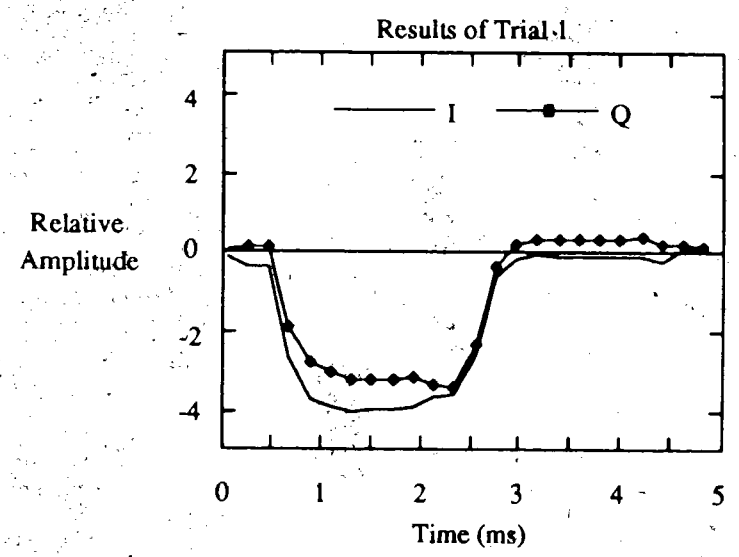

Figure 5.4: Beamformed results for the first trial.

5.4 Trial Number 2

For the second trial, the array was rotated so that the incident angle of the signal on the array was 30° as show in Figure 5.5. Figure 5.6 shows the complex envelopes

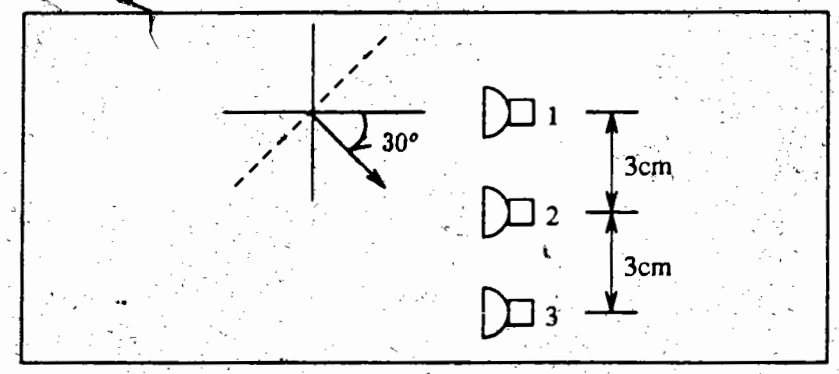

Figure 5.5: Hydrophone setup for the second trial.

for the three hydrophones and clearly illustrates the phase rotation. The processed signal is shown in Figure 5.7 where hydrophone 2 is taken as the reference point. All the delays are such that the signals lie on a plane perpendicular to the look direction and passing through hydrophone 2. To coherently combine the signals, the complex envelopes from hydrophones 1 and 2 were time shifted and rotated in phase. The beamformed signal resembles the signal from hydrophone 2, since that is the chosen time reference, and its magnitude is three times that of the signal from a single hydrophone.

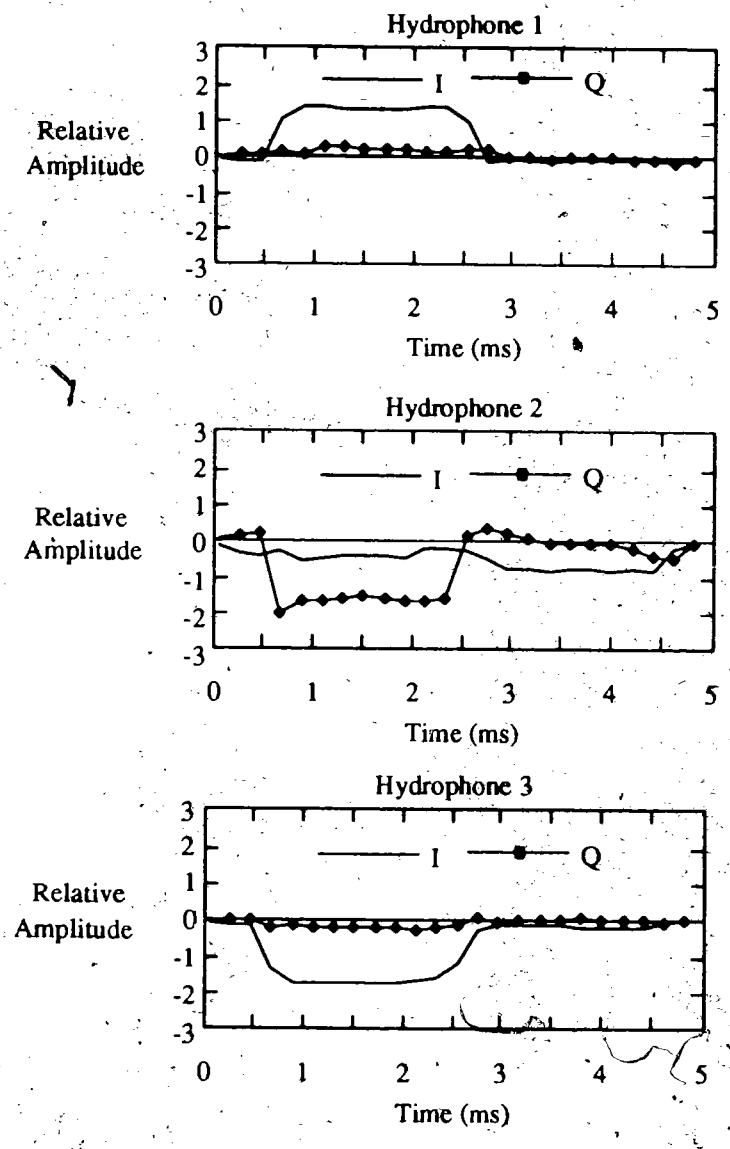

Figure 5.6: Demodulated signals from each of the hydrophones for trial 2.

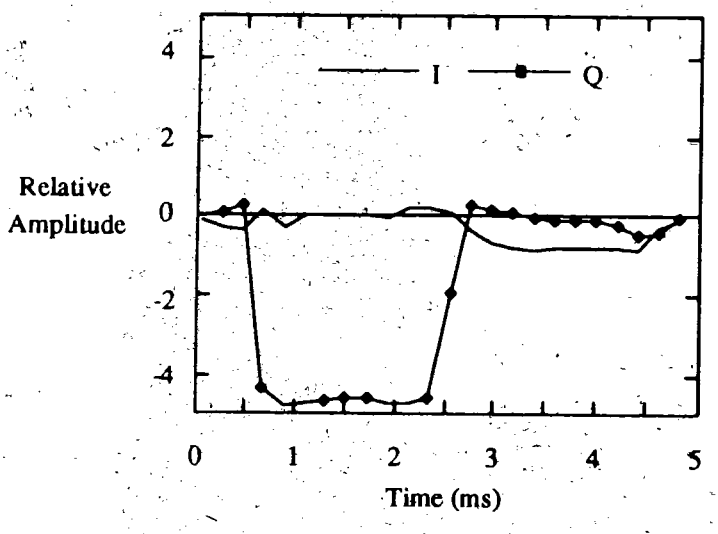

Figure 5.7: Beamformed results for trial 2.

5.5 Trial Number 3

For the final trial, two hydrophones were spaced 106 cm apart to demonstrate how the beamformer delays as well as phase rotates the complex envelope. A diagram of the setup is shown in Figure 5.8. Figure 5.9 shows the complex envelope from

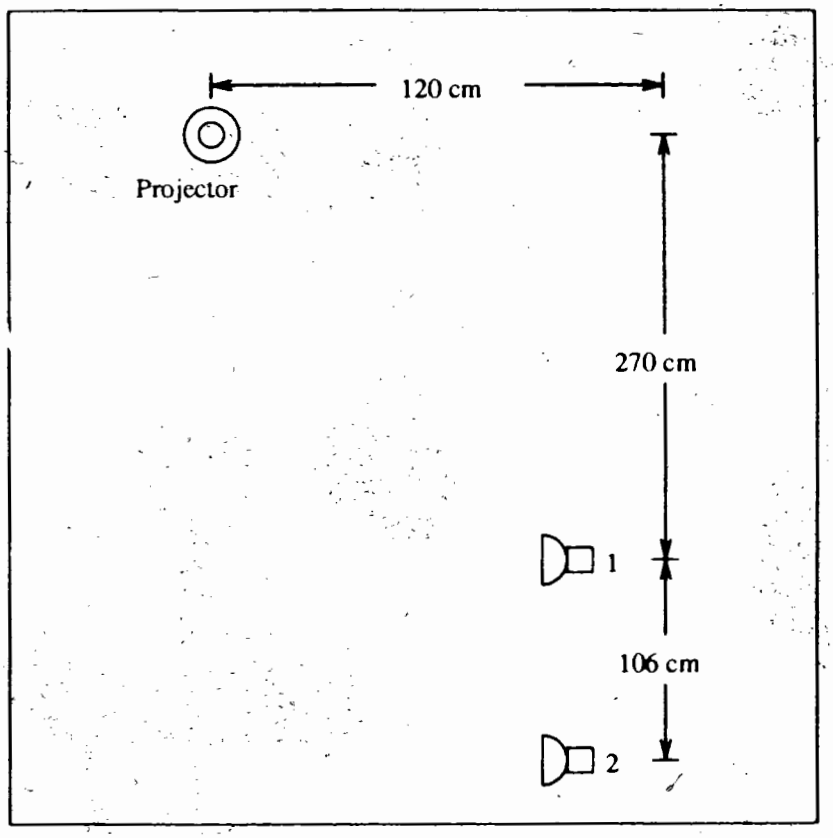

Figure 5.8: Hydrophone setup for the third trial.

each hydrophone. Not only is a phase rotation required but a time shift is obviously required if the signals are to add coherently. Figure 5.10 shows the signal after beamforming. Since hydrophone 1 was taken as the time reference point, the processed signal resembles that of hydrophone 1 and its magnitude is twice that of a single hydrophone.

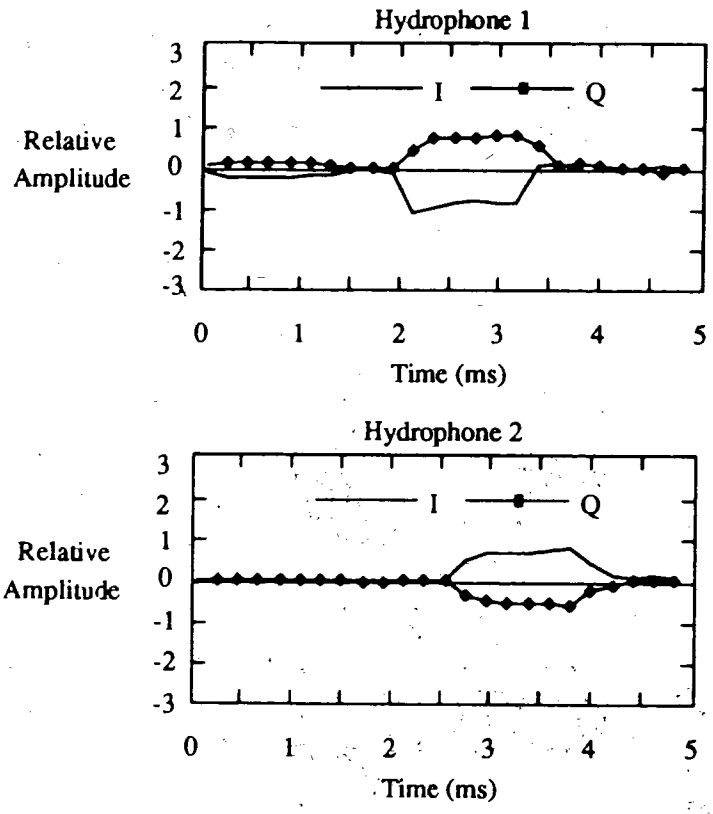

Figure 5.9: Demodulated signals from each of the hydrophones for the third trial.

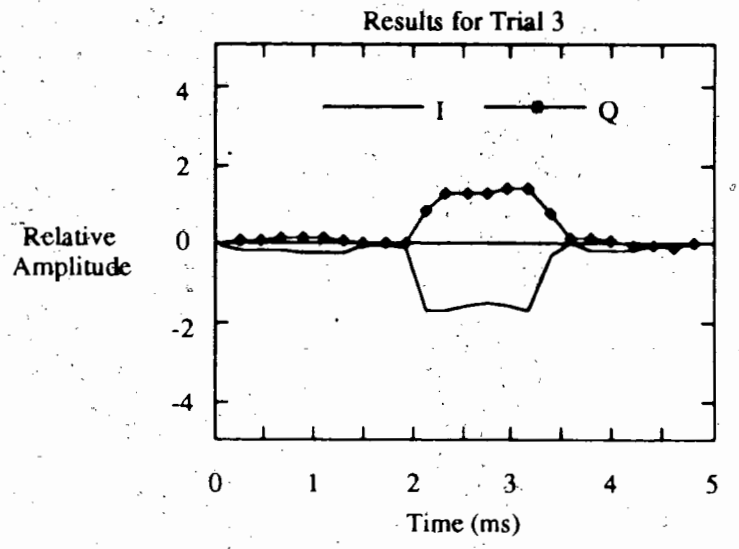

Figure 5.10: Beamformed results for the third trial.

It should be noted that in trials 1 and 2, the required time delays were small compared to the time required for a significant change in the complex envelope. Therefore, a simple phase rotation would have produced almost the same results. In trial 3, however, the delay was much longer and therefore both the time delay and phase shift had to be included. Figure 5.11 shows the result of only phase rotating the complex envelope for this setup. Because the complex envelopes do not overlap sufficiently in time, a distorted waveform results.

These trials demonstrated the new beamformer's validity and its advantage over a phase-rotation beamformer. For trial 1, the signal was broadside to the array and the beamformer simply had to add the complex envelope from each hydrophone. For trial 2, the incident angle of the signal on the array was 30°. To coherently combine the signal from each hydrophone, the beamformer had to phase rotate the complex envelopes before adding them together. For the first two trials, a phase-rotation beamformer would have been adequate since the time delays were small compared to the time required for a significant change in the complex envelope. For the third trial,

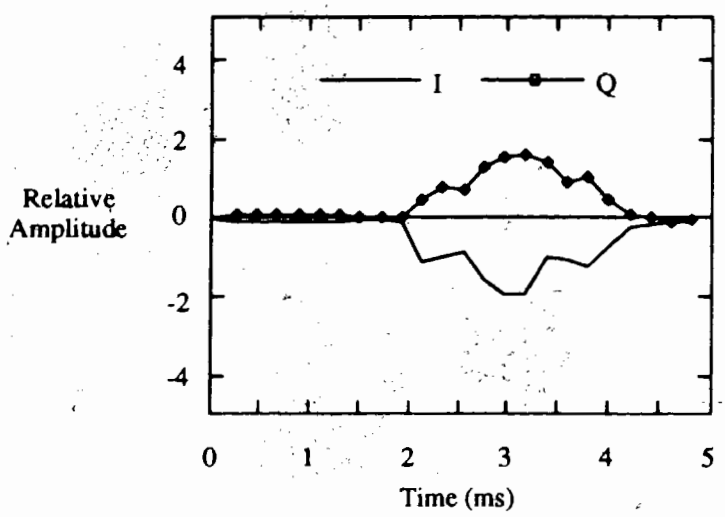

Figure 5.11: Results for Trial 3 when the complex envelope is rotated in phase only.

the delay was longer and a phase-rotation beamformer formed a distorted signal. By delaying the complex envelope, as well as phase rotating it, the new beamformer avoided the problem of the phase-rotation beamformer.

Chapter 6

Conclusion

Because of the severe attenuation of electromagnetic radiation in water, the acoustic channel is the only practical means for communicating with an AUV underwater. However, the acoustic channel is a reverberant environment resulting in a large amount of multipath interference. Using a hydrophone array reduces the effect of multipath interference by improving the spatial selectivity to incoming signals over that of a single hydrophone. The process by which the signals from an array of hydrophones are combined is known as beamforming. This thesis describes a true time delay bandpass beamformer which has several advantages over previous beamforming techniques for the specific application of communicating with an AUV and other applications as well.

Unlike FFT beamforming, the proposed beamforming technique easily handles arbitrary arrays, avoids edge effects and can produce a single continuously steerable beam.

The proposed beamforming technique also has advantages over previous time-domain beamforming techniques. The simplest time domain beamformers must grossly oversample the received signal in order to provide signal samples at the re-

quired time delays. The sampling rate can be reduced by using interpolation to realize the time delays, however, the bandpass signal must still be sampled at twice its highest frequency. Also, if the bandpass signal needs to be demodulated, a separate demodulator is required.

The new beamformer combines down conversion to complex baseband, time delay, and phase rotation into a single process. First, bandpass sampling is used to recover the complex envelope which eliminates the mixers and reduces the sampling frequency. Interpolation is then employed to time delay the complex envelope. It is shown that to coherently combine the complex envelopes from the hydrophones in an array, it is not sufficient to simply delay the complex envelopes but it is also necessary to rotate them in phase. The new beamforming technique is able to delay and phase rotate the complex envelopes using only a single FIR filter for each I and Q channel per hydrophone.

Several interpolation techniques were examined and compared. The one chosen minimized the mean squared error, for a white noise lowpass process, between the actual signal and the estimated signal and provided the best interpolation with the smallest number of filter taps. This interpolation technique requires that the signal's autocorrelation function be known for it to be optimum for the specific process. However, results were given that indicate the interpolation works well for signals whose statistics were not known or had changed over time if the signal is assumed to be a bandlimited white noise process.

The proposed beamforming technique was tested using data collected in Burrard Inlet with the underwater acoustic testbed. The results graphically demonstrate how the complex envelope from the various hydrophones need to be both delayed and phase rotated so that they can be coherently combined. Three trials were carried out using both a small and a large array. The small array consisted of three hydrophones spaced 3 cm apart. The beamformer was tested using the small array

when the incident angle of the received signal was 0° and 30°. For the third trial, two hydrophones were spaced 106 cm apart to demonstrate the necessity of delaying the complex envelope in addition to rotating the phase. This showed the inadequacy of simple phase-rotation beamformers when the complex envelope changes significantly over the length of the array.

The simple technique for time-domain beamforming developed in this thesis can be used for RF communications and radar as well as the underwater communications and sonar applications emphasized here.

Appendix A

Beamformer FIR Filter Coefficients Derivation

This appendix presents the mathematics for calculating the beamforming-filter coefficients, $\mathbf{v}_i$ and $\mathbf{w}_i$.

As explained in section 2.1.2, the complex envelope from each of the hydrophones must be time shifted by τ_i and then phase rotated before being added together. If τ_i is positive, then the signal is delayed and if τ_i is negative then the signal is advanced in time. If no delay is necessary, that is $\tau_i = 0$, then the FIR filters simply recover the complex envelope, which is described in section 3.2.3.

When $\tau_i = 0$, the time reference point where the quadrature components are interpolated at is halfway between an I sample and a Q sample. A new time delay, τ_{di}, is defined as

$$\tau_{di} = \tau_i - T_s/2 \tag{A.1}$$

which references the required delay to the I sample, as shown in Figure A.1. T_s is the bandpass sampling frequency. The delay is then normalized and divided into two

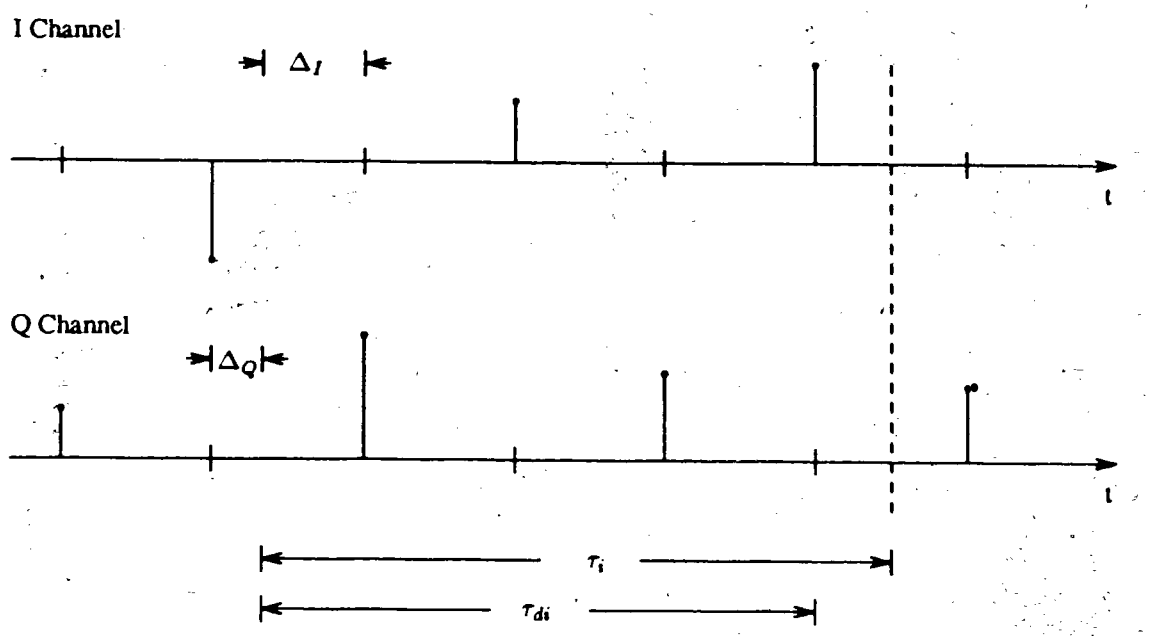

Figure A.1: I and Q samples and the various delays.

components

$$q_i = \frac{t_{di}}{T_s} = q_{INT_i} + q_{FRAC_i} \tag{A.2}$$

where q_{INT_i} is an integer and q_{FRAC_i} is a fraction, and both have the same sign.

Values for Δ, Figure A.1, can be calculated using q_{FRAC_i}. Two values exist, one for the I channel, Δ_I, and one for the Q channel, Δ_Q. The equation for Δ_I is

$$\Delta_I = \begin{cases} 1/2 - q_{FRAC_i}/2 & \tau_i \geq 0 \\ -1/2 - q_{FRAC_i}/2 & \tau_i < 0 \end{cases} \tag{A.3}$$

and for Δ_Q is

$$\Delta_q = \begin{cases} \Delta_I - 1/2 & \Delta_I \geq 0 \\ \Delta_I + 1/2 & \Delta_I < 0 \end{cases} \tag{A.4}$$

Assuming the sampling frequency is calculated using equation (3.8) so that the

sampled sequence is

$$\{\cdots, I, Q, -I, -Q, I, \cdots\}. \tag{A.5}$$

there are four cases to consider when calculating the filter coefficients.

- Beamforming Filter begins with a $+I$ sample
- Beamforming Filter begins with a $+Q$ sample
- Beamforming Filter begins with a $-I$ sample
- Beamforming Filter begins with a $-Q$ sample

It is important to recognize this point since it determines which of the filter coefficients must be sign inverted. If the beamformer filter's length is $2L$, then the following equations determine what sample the filter begins with.

- If $(q_{Int_i} + L)/4$ is an integer then filter begins with +I
- If $(q_{INT_i} + L + 1)/4$ is an integer then filter begins with +Q
- If $(q_{INT_i} + L + 2)/4$ is an integer then filter begins with -I
- If $(q_{INT_i} + L - 1)/4$ is an integer then filter begins with -Q

Note that the beamformer filter's length is a multiple of 4. Initially, the filters that interpolate the I and Q channel each had an even number of taps. Interleaving the interpolation filters to produce the beamforming filters ensures its size is a multiple of 4.

Consider the first case, that is the beamforming filter begins with a $+I$ sample. The filter coefficients used to interpolate the delayed quadrature components, $I_i(nT_o - \tau_i)$ and $Q_i(nT_o - \tau_i)$, are first calculated. This is nothing more than the interpolation

problem described in section 3.2.2. The equations for $\mathbf{a}_i$ and $\mathbf{b}_i$, used to interpolate the I and Q according to equations (4.1) and (4.2), are

$$\mathbf{a}_i = \mathbf{R}_I^{-1}\mathbf{r}_I \tag{A.6}$$

$$\mathbf{b}_i = \mathbf{R}_Q^{-1}\mathbf{r}_Q \tag{A.7}$$

where $\mathbf{r}$ is defined by equation (3.37) and $\mathbf{R}$ is defined by (3.38).

The coefficients calculated using equations (A.6) and (A.7) interpolate the delayed complex envelope when the sampled bandpass signal is divided into I samples and Q samples with the correct sign. The next step is to create two filters that interpolate the delayed complex envelope directly from the samples of the bandpass signal. This involves having to negate every second coefficient of $\mathbf{a}_i$ and $\mathbf{b}_i$ as well as interleaving 0s between the coefficients. Defining two $2LXL$ matrices $\mathbf{C}$ and $\mathbf{D}$ as

$$\mathbf{C} = \begin{bmatrix} 1 & 0 & 0 & \cdots & 0 \\ 0 & 0 & 0 & \cdots & 0 \\ 0 & -1 & 0 & \cdots & 0 \\ 0 & 0 & 0 & \cdots & 0 \\ 0 & 0 & 1 & \cdots & 0 \\ & & \vdots & & \\ 0 & 0 & 0 & \cdots & -1 \\ 0 & 0 & 0 & \cdots & 0 \end{bmatrix} \tag{A.8}$$

and

$$\mathbf{D} = \begin{bmatrix} 0 & 0 & 0 & \cdots & 0 \\ 1 & 0 & 0 & \cdots & 0 \\ 0 & 0 & 0 & \cdots & 0 \\ 0 & -1 & 0 & \cdots & 0 \\ 0 & 0 & 0 & \cdots & 0 \\ 0 & 0 & 1 & \cdots & 0 \\ & & \vdots & & \\ 0 & 0 & 0 & \cdots & 0 \\ 0 & 0 & 0 & \cdots & -1 \end{bmatrix} \tag{A.9}$$

two new $2LX1$ vectors, $\mathbf{a}_i'$ and $\mathbf{b}_i'$, can be calculated where

$$\mathbf{a}_i' = \mathbf{Ca} \tag{A.10}$$

and

$$\mathbf{b}_i' = \mathbf{Db} \tag{A.11}$$

Now the delayed complex envelope is calculated from the bandpass signal samples directly without having to separate the samples into I and Q samples and negate every second I and Q sample. The delayed quadrature components are

$$I_i(nTo - \tau_i) = \mathbf{a}_i'^T\mathbf{x} \tag{A.12}$$

$$Q_i(nTo - \tau_i) = \mathbf{b}_i'^T\mathbf{x} \tag{A.13}$$

where $\mathbf{x}$ contains the samples of the bandpass signal.

The final step to calculate $I_{Di}(nT_o)$ and $Q_{Di}(nT_o)$ is to rotate the phase of the delayed complex-envelope, equations (2.21) and (2.22). Using the filter coefficients $\mathbf{a}_i'$ and $\mathbf{b}_i'$, equations (2.21) and (2.22) can be expressed as

$$I_{Di}(nT_o) = \cos(\omega_c\tau_i)\mathbf{a}_i'^T\mathbf{x} + \sin(\omega_c\tau_i)\mathbf{b}_i'^T\mathbf{x} \tag{A.14}$$

$$= (\cos(\omega_c\tau_i)\mathbf{a}_i'^T + \sin(\omega_c\tau_i)\mathbf{b}_i'^T)\mathbf{x} \tag{A.15}$$

and

$$Q_{Di}(nT_o) = -\sin(\omega_c\tau_i)\mathbf{a}_i'^T\mathbf{x} + \cos(\omega_c\tau_i)\mathbf{b}_i'^T\mathbf{x} \quad (A.16)$$

$$= (-\sin(\omega_c\tau_i)\mathbf{a}_i'^T + \cos(\omega_c\tau_i)\mathbf{b}_i'^T)\mathbf{x} \quad (A.17)$$

The vectors $\mathbf{v}_i$ and $\mathbf{w}_i$ which calculate $I_{Di}(nT_o)$ using the bandpass signal samples, equations (4.6) and (4.12), are then

$$\mathbf{v}_i = \cos(\omega_c\tau_i)\mathbf{a}_i' + \sin(\omega_c\tau_i)\mathbf{b}_i' \quad (A.18)$$

$$\mathbf{w}_i = -\sin(\omega_c\tau_i)\mathbf{a}_i' + \cos(\omega_c\tau_i)\mathbf{b}_i' \quad (A.19)$$

Equations (A.18) and (A.19) assume that the beamformer filters begin with a $+I$ sample. If the filter begins with a $+Q$ sample, then the samples appear at the filter taps as

$$[Q, -I, -Q, I, Q, \cdots, -Q, I] \quad (A.20)$$

To interpolate $I_i(nT_o - \tau_i)$ and $Q_i(nT_o - \tau_i)$ directly from the signal samples, $\mathbf{a}_i$ must be multiplied by $-\mathbf{D}$ and $\mathbf{b}_i$ must be multiplied by $\mathbf{C}$ to ensure the samples are multiplied by the correct coefficients.

$$\mathbf{a}_i' = -\mathbf{D}\mathbf{a}_i \quad (A.21)$$

$$\mathbf{b}_i' = \mathbf{C}\mathbf{b}_i \quad (A.22)$$

Equations (A.18) and (A.19) are still used to calculate the beamformer filter coefficients $\mathbf{v}_i$ and $\mathbf{w}_i$.

For the third case when the filters begin with a $-I$ sample, the samples appear at the filter taps as

$$[-I, -Q, I, Q, -I, \cdots, I, Q] \quad (A.23)$$

This time both channels need to be negated so the equations for $\mathbf{a}_i$ and $\mathbf{b}_i$ are

$$\mathbf{a}_i' = -\mathbf{C}\mathbf{a}_i \quad (A.24)$$

$$\mathbf{b}_i' = -\mathbf{D}\mathbf{b}_i \tag{A.25}$$

and for the fourth case, the samples are

$$[-Q, I, Q, -I, -Q, \cdots, Q, -I] \tag{A.26}$$

and the Q channel needs to be negated

$$\mathbf{a}_i' = \mathbf{D}\mathbf{a}_i \tag{A.27}$$

$$\mathbf{b}_i' = -\mathbf{C}\mathbf{b}_i \tag{A.28}$$

Again, equations (A.18) and (A.19) are used to determine the beamforming coefficients for both cases.

If equation (3.10) is used to calculate the sampling frequency, the sampled data is

$$\{\cdots, I, -Q, -I, Q, I, -Q, \cdots\} \tag{A.29}$$

instead of

$$\{\cdots, I, Q, -I, -Q, I, \cdots\} \tag{A.30}$$

the difference being the Q channel has been shifted 180°. The same procedure as before is used to calculate the filter coefficients except now $\mathbf{b}_i$ must be multiplied by -1.

Bibliography

[1] I. R. Radziejewski, An Investigation of the Underwater Acoustic Communications Channel. *M.A.Sc. Thesis,* Simon Fraser University, Burnaby, B.C., July 1990

[2] W. S. Burdic, *Underwater Acoustic System Analysis,* Prentice-Hall, Englewood Cliffs, New Jersey, 1984, 322-359

[3] W. C. Knight, R. G. Pridham, and S. M. Kay, Digital Signal Processing for Sonar. *Proceedings of the IEEE,* **Vol. 69, No. 11** (Nov. 1981) 1451-1507

[4] R. F. W. Coates, *Underwater Acoustic Systems,* Macmillan Education Ltd., London,.England, 1990

[5] J. Catipovic, and L. Freitag, High Data Rate Acoustic Telemetry for Moving ROV's in a Fading Multipath Shallow Water Enviroment. *Proceedings of the OES Symposium on Autonomous Underwater Vehicle Technology,* (June 1990) 296-303

[6] D. E. Dudgeon, R. M. Mersereau, *Multidimensional Digital Signal Processing,* Prentice-Hall, Englewood Cliffs, New Jersey, 1984, 289-338

[7] D. E. Dudgeon, Fundamentals of Digital Array Processing. *Proceedings of the IEEE,* **Vol. 65, No. 6** (June 1977) 898-904

[8] R. F. Follett, High Resolution Broadband FFT Beamformer Simulation and Analysis. *Proceedings of the OES Symposium on Autonomous Underwater Vehicle Technology,* (June 1990), 254-259

[9] R. A. Mucci, Digital Beamformer Implementation Considerations. *IEEE EASCON,* (1981) 104-113

[10] G. L. Demuth, Frequency Domain Beamforming Techniques. *Proc. IEEE International Conference on Acoustics, Speech and Signal Processing*(1977) 713-715

[11] J. R. Williams, Fast Beam-Forming Algorithm. *J. Acoust. Soc. Am.*, **Vol. 44, No. 5** (1968) 1454-1455

[12] A. E. Cetin, and A. Rashid, Digital interpolation beamforming using recursive filters. *J. Acoust. Soc. Am.*, **Vol. 85, No. 1** (Jan. 1989), 493-495

[13] S. P. Pitt, T. Adams, and J. K. Vaughan, Design and implementation of a digital phase shift beamformer. *J. Acoust. Soc. Am.*, **Vol. 64, No. 3** (Sept. 1978) 808-814

[14] R. G. Pridham, and R. A. Mucci, Digital Interpolation Beamforming for Low-Pass and Bandpass Signals. *Proceedings of the IEEE*, **Vol. 67, No. 6** (June 1979), 904-919

[15] R. W. Schafer and L. R. Rabiner, A Digital Signal Processing Approach to Interpolation. *Proceedings of the IEEE*, **Vol. 61, No. 6** (June 1973)

[16] G. Oetken, T. W. Parks, and H. W. Schussler, New Results in the Design of Digital Interpolators. *IEEE Transaction on Acoustics, Speech, and Signal Processing*, **ASSP-23, No. 3** (June 1975) 301-309

[17] H. Liu, A. Ghafoor, and P. H. Stockmann, A New Quadrature Sampling and Processing Approach. *IEEE Transactions on Aerospace and Electronic Systems*, **Vol. 25, No. 5** (Sept. 1989), 733-748

[18] A. V. Oppenheim, and R. W. Schafer, *Digital Signal Processing*, Prentice-Hall, Englewood Cliffs, NJ, 1975

[19] L. J. Ziomek, *Underwater Acoustics A Linear Systems Theory Approach*, Academic Press, Orlando, Florida, 1985, 176-188

[20] A. Papoulis, *Probability, Random Variables, and Stochastic Processes*, McGraw-Hill Inc., New York, New York, 1965, 379-381

[21] C. M. Rader, A Simple Method fo Sampling In-Phase and Quadrature Components. *IEEE Transaction on Aerospace and Electronic Systems*, **AES-20** (Nov. 1984), 821-824

[22] D. W. Rice, and K. H. Wu, Quadrature Sampling With High Dynamic Range. *IEEE Transaction on Aerospace and Electronic Systems*, **AES-18** (Nov. 1982), 736-739

[23] W. M. Waters, B. R. Jarrett, Bandpass Signal Sampling and Coherent Detection. *IEEE Transaction on Aerospace and Electronic Systems*, **AES-18** (Nov. 1982), 731-736

[24] P. Bortot, Complex Demodulation Using Digital Technique. *INPUT Technical Reporting from ICS* **No. 2** (Dec. 1986)

[25] R. L. Mitchell, Creating Complex Signal Samples From a Band-Limited Real Signal. *IEEE Transaction on Aerospace and Electronic Systems,* **Vol. 25, No. 3** (May 1989), 425-427

[26] J. B. Marino, and E. Masgrau, Sampling In-phase and Quadrature Components of Band-pass Signals. *Signal Processing,* **Vol. 20, No. 2** (June 1990), 121-125

[27] W. L. Brogan, *Modern Control Theory,* 2nd Ed., Prentice-Hall, Englewood Cliffs, New Jersey, 1985, 324-327

[28] B. P. Lathi, Modern Digital and Analog Communication Systems, Holt, Rinehart, and Winston, Toronto, Ont., 1983

[29] H. Steyskal, Digital Beamforming Antennas. *Microwave Journal,* (Jan. 1987), 107-124

[30] R. G. Pridham, and R. A. Mucci, A novel approach to digital beamforming. *J. Acoust. Soc. Amer.,* **Vol. 63, No. 2** (Feb. 1978), 425-434

[31] D. F. Elliott, *Handbook of Digital Signal Processing,* Academic Press, San Diego, California, 1987, 173-286

[32] T. Horiguchi, A Digital Phase Delay Compensation Beam-Forming Scheme for Ultrasonic Imaging. *Japanese Journal of Applied Physics,* **Vol. 27, Supplement 27-1** (1988) 215-217

[33] B. D. Van Veen, and K. M. Buckley, Beamforming: A Versatile Approach to Spatial Filtering. *IEEE ASSP Magazine,* (April 1988), 4-24

[34] N. Boutin, Complex Signals: Part 1. *RF Design,* (Dec. 1989) 27-33

[35] N Boutin, Complex Signals: Part 2. *RF Design,* (Jan. 1990) 57-66

[36] N Boutin, Complex Signals: Part 3. *RF Design,* (March 1990) 109-115

[37] N Boutin, Complex Signals: Part 4. *RF Design,* (May 1990) 65-75

[38] R. A. Roberts, and C. T. Mullis, *Digital Signal Processing,* Addison-Wesley, Don Mills, Ont., 1987

[39] P. Rudnick, Digital Beamforming in the Frequency Domain. *J. Acoust. Soc. Am.,* **Vol. 46, No. 5** (1969) 1089-1090

[40] E. Brookner, Phased-Array Radars. *Scientific American*, **Vol. 252** (Feb 1985) 94-102

[41] H. J. Aiker, Mine Hunting Sonar. *Subnotes*, (Jan./Feb. 1990) 18-19

[42] M. J. Hinich, Beamforming when the sound velocity is not precisely known. *J. Acoust. Soc. Am.*, **Vol. 68, No. 2** (1980) 512-515